Access to follicular dendritic cells is a pivotal step in murine chronic lymphocytic leukemia B cell activation and proliferation

Heinig K., Gätjen M., Grau M., Stache V., Anagnostopoulos I., Gerlach K., Niesner R.A., Cseresnyes Z., Hauser A.E., Lenz P., Hehlgans T., Brink R., Westermann J., Dörken B., Lipp M., Lenz G., Rehm A., Höpken U.E.

Cancer Discovery
2014 DEC; 4: 1448-1465
2014 SEP 24 (first published online)
doi: 10.1158/2159-8290.CD-14-0096

Publisher: American Association for Cancer Research

Access to follicular dendritic cells is a pivotal step in murine chronic lymphocytic leukemia B cell activation and proliferation

Kristina Heinig[1], Marcel Gätjen[2], Michael Grau[3], Vanessa Stache[1], Ioannis Anagnostopoulos[4], Kerstin Gerlach[2], Raluca A. Niesner[5], Zoltan Cseresnyes[5,6], Anja E. Hauser[5,7], Peter Lenz[3], Thomas Hehlgans[8], Robert Brink[9], Jörg Westermann[10], Bernd Dörken[2,10], Martin Lipp[1], Georg Lenz[10], Armin Rehm[2,10]*#, and Uta E. Höpken[1]*#

[1]Max-Delbrück-Center for Molecular Medicine, MDC, Department of Tumor Genetics and Immunogenetics; 13125 Berlin, Germany
[2]Max-Delbrück-Center for Molecular Medicine, MDC, Department of Hematology, Oncology and Tumorimmunology, 13125 Berlin, Germany
[3]Philipps-University Marburg, Department of Physics, 35032 Marburg, Germany
[4]Charité-Universitätsmedizin Berlin, Department of Pathology, Campus Mitte, 10117 Berlin, Germany
[5]Deutsches Rheumaforschungszentrum, DRFZ, 10117 Berlin, Germany
[6]Max-Delbrück-Center for Molecular Medicine, MDC, Confocal and 2-Photon Microscopy Core Facility, 13125 Berlin, Germany
[7]Charité-Universitätsmedizin Berlin, 10117 Berlin, Germany
[8]Institute for Immunology, University Regensburg, 93042 Regensburg, Germany
[9]Garvan Institute of Medical Research, Darlinghurst NSW 2010, Australia
[10]Charité-Universitätsmedizin Berlin, Department of Hematology, Oncology and Tumorimmunology, Campus Virchow-Klinikum, 13353 Berlin, Germany

*Corresponding authors: Uta E. Höpken and Armin Rehm, Max-Delbrück-Center for Molecular Medicine, MDC, 13125 Berlin, Germany

e-mail: uhoepken@mdc-berlin.de; phone : +49-30-94063330; fax: +49-30-94063390

e-mail: arehm@mdc-berlin.de; phone : +49-30-94063817; fax: +49-30-94063124

# These authors contributed equally

Running Title: CXCR5 and lymphotoxin-dependent leukemia growth

The authors disclose no potential conflicts of interest.

Abstract

In human chronic lymphocytic leukemia (CLL) pathogenesis B cell antigen receptor signaling seems important for leukemia B cell ontogeny, whereas the microenvironment influences B cell activation, tumor cell lodging and provision of antigenic stimuli. Using the murine *Eμ-Tcl1* CLL model, we demonstrate that CXCR5-controlled access to follicular dendritic cells (FDCs) confers proliferative stimuli to leukemia B cells. Intravital imaging revealed a marginal zone B cell-like leukemia cell trafficking route. Murine and human CLL cells reciprocally stimulated resident mesenchymal stromal cells through lymphotoxin-β–receptor activation, resulting in CXCL13 secretion and stromal compartment remodeling. Inhibition of lymphotoxin/lymphotoxin-β-receptor signaling or of CXCR5 signaling retards leukemia progression. Thus, CXCR5 activity links tumor cell homing, shaping a survival niche, and access to localized proliferation stimuli.

Significance

CLL and other indolent lymphoma are not curable and usually relapse after treatment, a process where the tumor microenvironmemt plays a pivotal role. We dissect the consecutive steps of CXCR5-dependent tumor cell lodging and LTβR-dependent stroma-leukemia cell interaction, moreover, we provide therapeutic solutions to interfere with this reciprocal tumor-stroma crosstalk.

Introduction

In B cell chronic lymphocytic leukemia (B-CLL) patients, tumor cell survival and progression are linked to interactions between leukemia cells and non-tumor cells in microenvironments of the spleen, peripheral blood (PB), and bone marrow (BM) (1-3). Little is known about how CLL cells get access to a putative proliferation and survival niche within lymphoid organs, and a spatial and kinetic resolution of this process is desirable for two reasons. First, the microanatomy of B cell activation might illuminate the cellular encounters leading to apoptosis resistance versus proliferation induction in CLL cells. Second, signaling events could alter trafficking behavior of leukemia B cells, which is likely relevant for B cell stimulation.

B-CLL is the most frequent leukemia subtype affecting adults in western countries (4). It develops as an expansion of clonal mature $CD5^+$ B cells (5, 6), and gene expression profiles of CLL cells show that these malignant B cells resemble antigen-experienced memory B cells (7, 8). The precise cell-of-origin is debated. Depending on differentiation markers, or a putative antigen experience in conjunction with B cell receptor selection either a marginal zone (MZ) B-2 cell, a B-1 lymphocyte or a hematopoietic stem cell origin have been proposed (9, 10).

Several genomic aberrations involving karyotypic alterations or mutations in TP53, Notch1 and other markers are frequently reported in CLL cases (3, 11). High TCL1 (T cell leukemia/lymphoma 1) oncogene expression is linked to an aggressive B-CLL phenotype, with leukemic cells displaying a nonmutated immunoglobulin (Ig) receptor and profound ZAP70 expression (3, 12). A mouse B-CLL model has been developed by introducing a transgene encoding human *Tcl1* under the control of the IgH Eμ-enhancer, resulting in *Tcl1* overexpression at the mostly mature stages of B cell development (13). *Tcl1* transgenic mice develop B-CLL-like tumors characterized by an

expansion of $B220^{lo}IgM^{+}CD5^{+}CD11b^{+}$ cells, initially localized in the peritoneum, and subsequently in the spleen, BM, and PB. This B-CLL model has proven suitable to phenocopy several aspects of the human disease, including low proliferative progression, tissue distribution, and B cell differentiation status.

As in the migration of their normal cellular counterparts, trafficking and homing of CLL cells to and within the tissue microenvironment is regulated by adhesion molecules in concert with the chemokine-chemokine receptor system (14). The homeostatic chemokine receptor CXCR4 has emerged as a key receptor in the recruitment of and crosstalk between malignant B cells and their protective bone marrow microenvironment (15). Expression of secondary lymphoid organ (SLO)-homing receptors, including CCR7 and CXCR5, on human B cell non-Hodgkin and Hodgkin lymphoma correlate with their dissemination and tissue localization to and within specific SLO compartments (16, 17).

In B-CLL pathogenesis a predominant role of B cell receptor (BCR) signaling in CLL ontogeny has emerged (1). Furthermore, it remains still elusive how the microenvironment assumes a central role in B cell activation and survival. Here, we aimed to link the mechanisms of leukemia cell activation and the microenvironment dependence during CLL pathogenesis in *Eμ-Tcl1* mice. We intravitally visualized the CXCR5-mediated guidance of leukemic B cells towards splenic B cell follicles via a route normally taken by MZ B cells. In germinal center (GC) light zones, tumor B cells productively interacted with follicular dendritic cells (FDC), accelerating proliferation and clinical progression. Leukemia cells initiated LTαβ-dependent reciprocal crosstalk with resident follicular stroma cells, leading to CXCL13 release. Selective targeting of stroma-associated CXCL13 and LTβR-signaling abrogated this paracrine feedback-loop, hence retarding leukemia growth.

Results

CXCR5-dependent *Eμ-Tcl1* tumor cell localization within the growth-promoting environment of the splenic follicular compartment

To assess a putative role of CXCR5-governed leukemia cell migration and expansion in a CLL model, we crossed *Eμ-Tcl1* transgenic and *Cxcr5*$^{-/-}$ mice and followed their spontaneous tumor development compared to *Eμ-Tcl1* mice (Fig. 1A). We detected leukemia B cells (CD19^{+}CD5^{+}; Supplementary Fig. S1A-C and Fig. 1A) in the spleen and PB of *Eμ-Tcl1* mice after two months. In *Cxcr5*$^{-/-}$*Eμ-Tcl1* mice disease onset was substantially delayed. At 4-6 months of age, tumor cells in *Eμ-Tcl1* mice accounted for 30-50% of all lymphocytes, whereas tumor cells were barely detectable in *Cxcr5*$^{-/-}$*Eμ-Tcl1* mice. After >6 months, *Eμ-Tcl1* mice showed a further increased tumor load (>50%) in spleen and PB, whereas that in *Cxcr5*$^{-/-}$*Eμ-Tcl1* mice was still much lower. At 5–6 months of age, we also detected more leukemia B cells in the BM of *Eμ-Tcl1* compared to *Cxcr5*$^{-/-}$*Eμ-Tcl1* mice (Fig. 1A). *Eμ-Tcl1* leukemia cells in the spleen (Fig. 1B) expressed high levels of functional CCR7, CXCR4, and CXCR5 chemokine receptors, as shown *in vitro* by their migration in response to the respective chemokines CCL21, CXCL12, and CXCL13 (Fig. 1C). High expression levels of the homeostatic chemokine receptors were not restricted to the spleen, since LN, PB and BM derived leukemia cells also abundantly expressed CCR7, CXCR4 and CXCR5 (Supplementary Fig. S1D). Integrins β1, β2, β7, α4, and αLβ2 (LFA-1), were readily detected on all *Eμ-Tcl1* leukemia cells and quantitative real time PCR (qRT-PCR) revealed substantial expression for LTα, LTβ, and TNF-α in *Eμ-Tcl1* and *Cxcr5*$^{-/-}$*Eμ-Tcl1* cells (Supplementary Fig. S2A and B).

Hence, *Eμ-Tcl1* leukemia B cells are equipped with functional homeostatic chemokine receptors and integrins that enables them for access to SLOs.

We confirmed abundant high CXCR5 expression on human CLL tissue (Supplementary Fig. S2C) and on human peripheral CLL blood samples (Supplementary Fig. S2D). Much weaker expression was observed on CLL cells localized within proliferation centers (PC), which are thought to harbor a proliferative fraction of CLL leukemia B cells (18).

Next, malignant B cells derived from diseased *Eμ-Tcl1* or *Cxcr5*$^{-/-}$*Eμ-Tcl1* mice were adoptively transferred into Wt congenic recipients. After 72 hrs, leukemia cells were detected in the spleen, PB, and BM. *Eμ-Tcl1* cells were predominantly localized within splenic B cell follicles (Fig. 1D). In contrast, *Cxcr5*$^{-/-}$*Eμ-Tcl1* cells were completely absent from B cell follicles, and were mostly found in the MZ outside the metallophilic macrophage ring (MOMA-1^{+}). To further assess whether this follicular localization had any consequences on leukemia progression, we applied a CXCL13 antibody to inhibit CXCR5 signaling. Expansion of adoptively transferred tumor B cells was substantially diminished in spleens of CXCL13-treated mice (Figure 1E).

Collectively, these data indicate that CXCR5 contributes to accelerated leukemia development, potentially by conferring a survival advantage to *Eμ-Tcl1* tumor cells within the B cell follicle.

Gene expression signatures indicate a proliferative advantage in CXCR5-expressing *Eμ-Tcl1* leukemia compared with *Cxcr5*$^{-/-}$*Eμ-Tcl1* leukemia

The slower kinetics of tumor growth in *Cxcr5*$^{-/-}$*Eμ-Tcl1* transgenic mice could relate to a reduced proliferation rate. Using genome-wide expression arrays, we examined relative changes in gene expression of splenic leukemia cells derived from diseased *Eμ-Tcl1* versus *Cxcr5*$^{-/-}$*Eμ-Tcl1* mice. Gene set enrichment analysis (GSEA) identified seven different proliferation signatures that discriminated *Cxcr5*$^{+/+}$ from *Cxcr5*$^{-/-}$ leukemias

(Fig. 2A and B; Supplementary Fig. S3A). For example, the gene-expression signature of the neighborhood of the CDC2 cell division cycle 2 (G1 to S and G2 to M) in the GNF2 expression compendium (19) predicted a proliferative advantage in CXCR5-expressing *Eμ-Tcl1* tumor cells and included genes involved in cell cycle regulation, DNA synthesis, and protein translation. Conversely, $CXCR5^{-/-}$ versus $CXCR5^{+/+}$ leukemia did not differentially express gene sets of apoptosis-mediating pathways like the KEGG apoptosis signature (20) (Fig. 2C).

Eμ-Tcl1 leukemia B cells represent the unmutated and aggressive type of B-CLL (21). A bias towards the restricted use of V_H gene segments was noted, indicating that the expanded $CD5^+$ B cell population in *Eμ-Tcl1* mice could be derived from B-1 lineage cells. We performed a transcriptome analysis of leukemia cells, murine B-1 B and MZ B cells (Fig. 2D and E). Two gene expression signatures comprised of the top 100 downregulated and upregulated genes in B-1 cells compared to MZ B cells were defined. When gene expression of these signatures was compared in leukemia cells and in follicle cells derived from Wt mice, a strikingly higher similarity of *Eμ-Tcl1* leukemia cells to B-1 B cells as compared to MZ B cells was revealed.

Next, we adoptively transferred leukemia cells to synchronize pathogenic events at the onset of the disease (22). Leukemia cells were retrieved and we used RT-qPCR to assess their gene expression pattern, focusing on genes reportedly involved in CLL survival (23). Wnt6 and Wnt10a were modestly elevated in *Eμ-Tcl1* tumor cells, whereas *$Cxcr5^{-/-}$Eμ-Tcl1* leukemia cells showed substantially higher gene expression for the transcription factor Runx2 (Supplementary Fig. S3B). The cell cycle inhibitor p21, a transcriptional target of Runx2 (24), was also upregulated in *$Cxcr5^{-/-}$Eμ-Tcl1* leukemia (Supplementary Fig. S3C), indicating that CXCR5 confers *Eμ-Tcl1* tumor cells with a proliferative advantage.

When leukemia cells were co-cultured with the FDC/HK cell line, the activities of serine/threonine kinases p42/p44, p38 and Akt were indiscriminable in both genotypes (Supplementary Fig. S3D). Additionally, a comparable proliferation rate of Wt and CXCR5-deficient tumor cells was detectable when leukemia cells were co-cultured with the stroma cell line M2-10B4 (Fig. 2F). This indicates that when tumor cells get access to stromal cell support *in vitro*, their proliferation is supported. *In vivo*, CXCR5 controls this access to a tumor growth-promoting stromal niche.

Eμ-*Tcl1* leukemia cells move directly across the MZ-WP border to gain access to the B cell follicle

Lymphocyte transition from the blood into the spleen occurs at the MZ. Follicular B cells and T cells then migrate along the FRC-rich MZ bridging channels (MZBC) toward the splenic white pulp (WP) and eventually enter the periarteriolar lymphoid sheaths (PALS). This movement is largely CCR7-dependent(25). In contrast, MZ B cells undergo CXCR5- and S1P1-controlled constitutive shuttling between the MZ and the follicle (26).

It is unknown how CLL cells access the B cell follicle. Applying a sequential static imaging approach, SNARF-1-labeled tumor or B cells were adoptively transferred into B6 recipients. One to 5 hrs later, spleens were stained with anti-B220 to locate B cell follicles and anti-MOMA-1 to highlight the border between WP and MZ (Fig. 3A and 3B). We counted the numbers of labeled *Eμ-Tcl1* leukemia cells or normal B cells in four regions of the spleen: the RP (MOMA-1$^-$B220$^-$), MZ (MOMA-1$^+$B220$^+$), B cell follicle (MOMA-1$^-$B220$^+$), and T/B zone interface (Fig. 3A and 3B). One hour after transfer, normal B cells were found predominantly in the RP but also in the MZ (Fig. 3B and 3C), while >50% of tumor cells were either localized within the MZ or in B cell follicles (Fig.

3A and 3C). Two hours after transfer, B cells were still predominantly located in the RP, with a smaller proportion in the MZ, and single B cells appeared at the T/B cell border. Tumor cells were equally distributed between MZ and B cell follicle with a smaller proportion in the RP. Three to 5 hrs after transfer, the proportion of leukemia cells in B cell follicles further increased whereas tumor cells remained absent from the T/B cell border (Fig. 3A-3D). In contrast, B lymphocytes transiently accumulated at the T/B zone border (between 2-3 hrs) before entering the B cell follicle (3-5 hrs; Fig. 3B-3D).

The positioning of B cells at the T/B cell border is regulated by CCR7 and EBI2 chemotactic activity (27). After adoptive transfer, both *Ccr7*$^{-/-}$ and *Ccr7*$^{+/+}$ leukemia cells showed the same direct migratory route from the MZ into B cell follicles, with an accumulation at the FDCs (Supplementary Fig. S4A). Likewise, *Ebi2*$^{-/-}$*Eμ-Tcl1* cells exhibited the same localization behavior (Supplementary Fig. S4B and C). Clinically, spontaneous leukemia development in *Ebi2*$^{-/-}$*Eμ-Tcl1* double-transgenic animals compared to *Eμ-Tcl1* mice revealed no alteration in tumor growth (Supplementary Fig. S4D).

In summary, *Eμ-Tcl1* leukemia B cells directly cross the MZ sinus, reaching the B cell follicle faster than follicular B cells, and this process is tightly regulated by the CXCL13/CXCR5 signaling axis.

Eμ-Tcl1 leukemia cells tightly co-localize with the follicular FDC network and exhibit strong ZAP-70/Syk and BTK activity

FDCs reside within primary follicles and in the GC light zone of secondary B cell follicles. They express CXCL13, which enables CXCR5-expressing B cells to migrate into lymphoid follicles. Since a strong correlation has been proposed between antigen-stimulated BCR signaling and the clinical course of CLL, we identified follicular stromal

networks that locally interact with *Eμ-Tcl1* leukemia cells. Eight hrs after transferring leukemia cells, tumor cells tightly intermingled with FDCs (Fig. 4A). These cells stained strongly for the proliferation marker Ki67 ($CD45.2^{+}Ki67^{+}$), indicating a proliferation-driving interaction. 77.5 ± 5.8% of all $Ki67^{+}$ leukemia cells were tightly associated with the FDC networks, whereas only 22.1 ± 3.6% of follicular $Ki67^{+}$ leukemia cells were located outside of the FDC networks (Fig. 4B).

Next, we simultaneously injected differentially labeled follicular B cells ($B220^{+}CD21^{int}CD23^{hi}$) with *Eμ-Tcl1* leukemia cells and quantified the proportion of transferred cells within the FDC-rich zone (Fig. 4C). Less than 50% of all transferred follicular B cells were found at the FDC networks. In contrast, more than 70% of leukemia cells strongly co-localized with FDCs (Fig. 4D).

Consistent with the animal model, FDCs could be detected in human CLL specimen at variable rates and shapes, ranging from distinct reticular forms to more complex networks (Supplementary Fig. S5).

Leukemic cells of patients with progressive CLL express the protein tyrosine kinase ZAP-70, which is functionally associated with increased BCR signaling (28). Another tyrosine kinase that is uniformly overexpressed and constitutively active in CLL is Bruton's tyrosine kinase (BTK) (29-31). Here, employing an antibody that crossreacts with phosphorylated (p)-ZAP-70 and p-Syk (32), we showed substantially enhanced expression of p-ZAP-70/Syk in *Eμ-Tcl1* leukemia cells compared with B lymphocytes. This finding was corroborated with a p-BTK antibody (Fig. 4E and F), indicating that *Eμ-Tcl1* leukemia cells exhibit increased BCR activity.

BCR engagement and growth factor supply could depend on the environmental context. Here, tissue-resident leukemia cells from the spleen showed an enhanced proportion of cells in S phase ($BrdU^{+}$), suggesting a stronger stimulus in SLOs compared

to cells derived from PB (Fig. 4G). Thus, *Eμ-Tcl1* leukemia cell contacts to FDC networks could be a prerequisite for tumor cell proliferation which is enhanced by BCR signaling and local cytokine provision.

To further dissect these mechanisms, we co-cultured seven different *Eμ-Tcl1* leukemia cell clones in the presence of FDC/HK cells (33). When HK cells were prestimulated with LTα1β2, an almost twofold higher survival rate of leukemia cells as compared with HK cells alone was seen. This indicated that engagement of the LTβR could induce provision of B cell growth factors (Fig. 4H). Next, we mimicked cytokine and growth factor conditions that were suggested to support either GC B cell proliferation or follicular B cell lymphoma expansion (34, 35). When supplemented, a substantial increase in cell proliferation was obtained for BAFF, CXCL12, Sonic hedgehog (SHH), hepatocyte growth factor (HGF), CXCL13, and IL-15 (Fig. 4H). Employment of the γ-secretase inhibitor DAPT, and thus Notch pathway blockade, served as a negative control. To discriminate between an anti-apoptotic effect and a proliferation induction, we repeated this assay for selected cytokines and measured instead BrdU uptake. We observed enhanced proliferation rates of *Eμ-Tcl1* leukemia cells ($BrdU^+$) after stimulation with LTα1β2 and an even stronger proliferation in the presence of IL-15 (Fig. 4I). Treatment of cocultures with the CXCR4 antagonist AMD3100 inhibited BrdU uptalke (Fig. 4I), which supports the notion that the CXCR4 signaling directly stimulates proliferation of CLL cells. Inclusion of the Gαi/o-protein inhibitor pertussis toxin (PTX) considerably diminished leukemia B cell viability in HK cocultures (Supplementary Fig. S6A). Hence, BrdU uptake could not be reliably determined because of the predominant fraction of apoptotic leukemia cells.

In accordance, when human CLL cells were cocultured with FDC/HK cells, enhanced proliferation of CLL cells was also observed and could be further enhanced by

adding Il-15 (Supplementary Fig. S6B). Prestimulation with LTα1β2 had a modest effect, which might be explained by higher endogenous expression of LTα and LTβ in human CLL cells (Figure 7E).

If antigen recognition is important for *Eμ-Tcl1* leukemia cell growth then restricting the antigen specificity of leukemia cells against an irrelevant antigen might reduce their fitness *in vivo*. We generated *Eμ-Tcl1* x BCR^{HEL} double-transgenic mice and analyzed them after repetitive immunization with the cognate antigen HEL or without (Supplementary Table S1 and S2) for the development of a clonal B-CLL-like disease. Leukemia cell development equipped with the cognate BCR^{HEL} could not be observed in non-immunized or HEL-immunized mice, indicating that sole stimulation of the BCR^{HEL} does not confer sufficient signaling to promote *Eμ-Tcl1* leukemia development.

The dynamics of *Eμ-Tcl1* leukemia cell localization in the $CD21^{+}CD35^{+}$ GC light zone

The localization of *Eμ-Tcl1* tumor cells near FDCs suggested that this network might provide the combined chemoattractant, nutritive and antigenic stimuli for BCR engagement. To visualize the dynamic behavior of *Eμ-Tcl1* leukemia cells in relation to FDCs, we injected Alexa Fluor 568-conjugated anti-CD21/CD35 Fab-fragments for intravital FDC staining (Supplementary Fig. S7), together with CFDA-labeled *Eμ-Tcl1* leukemia or B cells. During a 30-min imaging period, we tracked individual motile Eμ-*Tcl1* leukemia cells or B cells that were localized within the B cell follicle or close to the FDCs for as long as the cells remained within the z stacks (height: 40–50 μm) of optical sections (Movie S1 and S2). Tracks of motile leukemia or B cells were also projected onto an image of the entire z stack, representing a midpoint in the imaging time period

(Fig. 4J). We could distinguish between a more stationary FDC-associated and a more motile follicular-located leukemia cell population based on total displacement from their origin (Fig. 4K), track velocity (Fig. 4L), and total track length (Fig. 4M).

All three parameters were substantially decreased when leukemia cells were close to the FDC networks, as opposed to those located within the outer B cell follicle (Fig. 4K-M; Fig. 4J, upper panel, and Supplementary Movie S1). This association was also obtained in follicular B cells (Figure 4K-M and Supplementary Movie S2), but fewer B cells were associated with FDCs (Fig. 4D and 4J, lower panel). We conclude that the decreased displacement rate and increased interaction time of leukemia B cells with FDCs could result from the tumor cells' cognate nature and their ability to encounter antigen-laden FDCs.

To assess follicular *Eμ-Tcl1* leukemia positioning following the organization of GCs into dark and light zones, we immunized B6 mice with sheep red blood cells. GC B cell positioning in the dark zone is crucially dependent on high CXCR4 expression (36). SNARF-1-labeled tumor cells were i.v. transferred; 8 hrs later, splenic sections were stained for PNA^+ GCs (centroblasts; dark zone), $CD21^+CD35^+$ FDC networks (light zone), and IgD^+ B cell follicles (Fig. 5A). Tumor cells were also pre-treated with the CXCR4 antagonist AMD3100 (Fig. 5B-D). *Eμ-Tcl1* leukemia cells localized exclusively in the $CD21^+CD35^+$ GC light zone, independently of CXCR4-signaling inhibition (Fig. 5B). Inhibition of CXCR4-signaling after AMD3100 treatment was confirmed *in vitro* in a chemotaxis assay (Fig. 5D).

The sphingosine-1-phosphate receptor S1P2 helps to confine B cells to the GC (37). GC B cells showed the highest gene expression of *S1pr2*. In contrast, *Eμ-Tcl1* leukemia cells exhibited low *S1pr2* expression comparable to the amounts of *S1pr2* in

MZ B cells (Fig. 5E). Collectively, *Eμ-Tcl1* leukemia cells are predominantly recruited to the $CD21^{+}CD35^{+}$ GC light zone, but they do not access the PNA^{+} dark zone.

In irradiated mice *Eμ-Tcl1* leukemia cells exhibit enhanced proliferation in close proximity to FDCs

Clinically, an unresolved problem in the treatment of indolent lymphoma is their propensitiy to relapse and to develop progressively chemo-resistance. The close association of *Eμ-Tcl1* leukemia cells with FDCs raised the question whether tumor cells might reciprocally support or initiate stroma cell network differentiation. To analyze the mechanisms of a putatively stroma-regulated treatment failure, we first assessed the stroma-inducing capacity of tumor cells in *Rag2*$^{-/-}$ mice that are devoid of mature lymphocytes and lack FRCs and FDCs. These mice still have MAdCAM-1^{+} marginal reticular cells (MRC), which produce CXCL13 and express the LTβR. Over a twenty-one day observation period, *Eμ-Tcl1* leukemia cells induced formation of follicular-like CXCL13-expressing FDC ($CD21^{+}CD35^{+}$) networks in *Rag2*$^{-/-}$ mice (Supplementary Fig. S8A). Leukemia-loaded spleen also upregulated CXCL13 und LTβ gene expression (Supplementary Fig. S8B).

Radiotherapy eliminates hematopoietic cells whereas mesenchymal stromal elements survive. To assess whether residual leukemia cells could exploit stromal contacts and engage with FDCs and MRCs, we transferred *Eμ-Tcl1* cells into irradiated congenic recipients. While essentially all benign $B220^{+}$ B cells were depleted after 48 hrs, FDCs persisted and the MRC ring expanded (Fig. 6A; upper left). Transferred CLL cells accumulated around the FDC networks in an even stronger manner than in untreated mice (Fig. 6A; lower panel). Functionally, transfer into irradiated hosts conferred tumor cells with an enhanced proliferative capacity (Fig. 6B and C), and the rate of tumor cells

in close proximity to FDC networks that stained strongly for Ki-67 was substantially higher compared to untreated controls (Fig. 6B). Irradiation of mice substantially enhanced splenic BAFF gene expression about 4-fold, whereas APRIL was weaker upregulated (Fig. 6D). We confirmed expression of the corresponding cytokine receptor BAFFR on leukemia cells (Fig. 6E).

To demonstrate that irradiation enhances proliferation in a BAFF dependent manner, we transferred tumor cells together with a blocking anti-BAFF antibody into irradiated mice. Treatment with the anti-BAFF antibody completely abrogated irradiation-induced proliferation in *Eμ-Tcl1* tumor cells (Fig. 6F).

Taken together, CLL cells are recruited to mesenchymal stromal cells, which in turn promote chemokine-mediated tumor cell attraction, growth acceleration through BCR stimulation and paracrine provision of cytokines.

Stromal LTβR-signaling is crucial for maintaining FDC structures and accelerates Eμ-*Tcl1* leukemia progression

FDC stimulation with cell-bound LTαβ or soluble LTα/TNFR1 agonist can induce the expression of CXCL13 and other cytokines (38). Since the leukemia cell itself was also a source of lymphotoxin (Supplementary Fig. S2B), we hypothesized that leukemia cell-associated LTαβ conferred the ligand for LTβR activation on FDCs and MRCs. To assess this regulatory feedback-loop, we inhibited LTαβ-LTβR signaling in *Eμ-Tcl1* mice using a LTβR-Ig fusion protein. Spontaneously diseased *Eμ-Tcl1* mice with a 5–15% tumor load in PB were treated with the decoy receptor protein LTβR-Ig. *Eμ-Tcl1* mice treated with a control Ig showed a substantially increased tumor load in PB from day 0 to day 38 of treatment, whereas no such increment was observed in LTβR-Ig-treated mice (Fig. 7A). Tumor load in the spleen of isotype-treated *Eμ-Tcl1* mice was

also higher than in LTβR-Ig-treated animals (Fig. 7B). Immunohistology showed substantial FDC disappearance (Fig. 7C) and a severe disturbance of MAdCAM-1^+ and BP-3^+ B cell follicle stromal structures (Supplementary Fig. S9A) in LTβR-Ig-treated animals. Splenic *Ccl21* and *Cxcl13* gene expressions were lower in LTβR-Ig-treated *Eμ-Tcl1* mice compared to controls (Fig. 7D).

Supporting a pathogenic role of LTβR-signaling, disease onset and progression was substantially delayed in *Lt*$\alpha^{-/-}$*Eμ-Tcl1*-double transgenic mice compared to *Eμ-Tcl1* animals (Supplementary Fig. S9B). Hence, tumor cell production of LTα accelerates tumor growth. Conversely, interference with LTβR signaling leads to growth reduction in a murine CLL model.

In line with the data from *Eμ-Tcl1* mice, lymphotoxin and TNFα transcripts could be detected in sorted human CLL cells, normal B cells, and in the human B-CLL line MEC-1 (Fig. 7E). Adoptive transfer of MEC-1 cells into *NOD/SCID/c-*γ*-chain*$^{-/-}$ mice elicited a follicular-like FDC network (Fig. 7F, left), a process which could be completely abrogated by LTβR-Ig-treatment (Fig. 7F, right). Thus, LTβR-signaling is an essential part of the reciprocal relationship between leukemia B cells and mesenchymal stromal cells.

Discussion

In the present study, we tracked the trafficking routes of murine CLL cells into protective microenvironmental niches in SLOs, and identified FDCs as a crucial resident stromal cell population that supports consecutive steps of leukemia pathogenesis. Using the *Eμ-Tcl1* transgenic mouse (13) as a CLL model, we also obtained functional evidence that the chemokine receptor CXCR5 has a dominant role in leukemia cell microanatomical localization.

Eμ-Tcl1 B cells showed a hierarchy among expressed homeostatic chemokine receptors. CXCR4 has been identified as a survival factor in CLL (39) and as an important homing receptor of neoplastic B cells to the BM (40), while CXCR5 expression is predominantly associated with CLL positioning in SLOs (41). Although CXCL12-CXCR4 engagement accelerates human B-CLL and murine *Eμ-Tcl1* leukemia cell proliferation *in vitro*, *in vivo* this activity requires access to a CXCL12 providing niche. In our murine CLL model, CXCR5 crucially controls homing of leukemia cells into the B cell follicles of SLOs. CXCR4 could not compensate for CXCR5 deficiency regarding their migratory functions: CXCR5-deficient leukemia cells were restricted to the MZ zone but not attracted to the B cell follicle, and tumor cells remained absent from the dark zone of the GC, the attraction to which is CXCL12-CXCR4 governed (36).

In the absence of CXCR5, spontaneous onset of disease in *Eμ-Tcl1* mice was severely delayed. Gene expression profiling uncovered a proliferative advantage in CXCR5-expressing *Eμ-Tcl1* tumor cells, while no obvious differences were found in apoptosis-mediating pathways. In conjunction with a compartment-specific higher proliferation rate, this observation is in line with the view that B-CLL is not a static or accumulative disease that simply results from long-lived lymphocytes defective in apoptosis (42, 43).

Migration of normal B cells toward follicles is mediated by the CXCL13-CXCR5 signaling axis and a stromal cell network (25, 44). CXCL13, which is produced by the FDC network and MRCs, guides circulating naive B cells in the proximity of FDCs, a prerequisite for the formation of B cell follicles (36). Moreover, CXCR5 also plays a unique role in trafficking and homing of B-1 B cells (45). In CLL patients, leukemia cells express high levels of functional CXCR5 and significantly higher CXCL13 serum levels were found compared to healthy controls (41).

With regard to these correlative studies in CLL patients, we aimed to dissect the CXCR5-dependent spatial positioning of *Eμ-Tcl1* leukemia cells *in vivo*. We found that upon adoptive transfer, *Eμ-Tcl1* leukemia cells lodged within the splenic B cell follicles in close proximity to FDCs. In sharp contrast, $CXCR5^{-/-}$ leukemia cells accumulated in the MZ of the spleen. Bajénoff and colleagues (46) showed that T and B lymphocytes are guided by FRCs and enter the WP across MZBCs. Here, we observed that *Eμ-Tcl1* leukemia cells directly crossed the MZ sinus and reached the B cell follicle faster than follicular B cells. Hence, leukemic cells exhibited remarkable functional similarity to MZ B-2 lymphocytes, which also shuttle directly from the MZ to the B cell follicle (26). Gene expression profiling revealed a higher similarity of *Eμ-Tcl1* leukemia cells with B-1 B cells, as compared to MZ B cells. This result is consistent with the initial classification of these tumors (47), and would also fit with several properties of the human unmutated variant of B-CLL. Although physiological differences between murine and human B cell populations exist prohibiting definitive conclusions (48), similarities are also appreciated that affect structural restriction of the BCRs, the poylreactivity towards autoantigens, expression of CD5, and the presentation as activated antigen-experienced B cells (3, 9, 49). B-1 cells can induce and associate with FDCs in mice, however trafficking routes of these cells have not been thoroughly analyzed (50).

CXCL13/CXCR5 signaling is crucial for B cell migration under steady-state conditions and enhances antigen encounter and BCR-triggered B cell activation (51). A strong correlation has been proposed between antigen-stimulated BCR signaling and the clinical course of CLL (3). An involvement of a microbial-derived or autoantigen component in the heavy chain Ig repertoire selection has been suggested in many CLL cases, leading to the occurrence of stereotyped BCRs (1, 52). Alternatively, a BCR-mediated antigen-independent, cell-autonomous signaling mechanism might account for CLL signaling activity. However, this *in vitro* model does not rule out involvement of in vivo extrinsic antigens as additional enhancers (53).

How could *Eμ-Tcl1* leukemia B cells receive proliferation stimuli in vivo? Using two-photon microscopy, we found that *Eμ-Tcl1* leukemia cells showed decreased displacement rates and increased interaction times with follicular FDCs compared to leukemia cells outside this area. This could result from their cognate nature and ability to encounter antigen-laden FDCs. The preferred tumor cell localization in the FDC-rich GC light zone may also be due to the paracrine provision of growth-promoting factors (34, 35). BCR engagement, as evidenced by activated BTK, and the receipt of growth factors could act differentially during tumor ontogeny and in a complementary manner. In this view, a strong antigen dependence exists in early stages, followed by a competition for natural ligand availability, then acqusition of additional oncogenic lesions and finally, selection for mutants that can co-opt autonomous signaling either from the BCR or their downstream effectors (54).

The differentiation of FDCs is essential for SLO organogenesis (55) and final FDC maturation crucially requires lymphoid tissue-inducer (LTi) cells and B cells expressing LTαβ (56). Consistent with previous reports that B-2 and B-1 B cells can induce the formation of mature FDC networks (50, 57), a human leukemia cell line

efficiently induced FDC networks in *NOD/SCID/c-γ-chain*$^{-/-}$ mice. This implies that B leukemia cells themselves provide the crucial factors for FDC differentiation in vivo. The crosstalk between leukemic B cells and rudimentary stromal cells could be of relevance for a post-therapeutic minimal residual disease state. Irradiation of Wt mice elicited an accumulation of leukemia B cells around radio-resistant FDCs and MRCs. This spatial proximity accelerated the growth rate of the tumor cells, most likely through an uncompeted access to FDCs.

Notably, much of the cellular proliferation in human CLL arises in pseudofollicular proliferation centers (PC) in SLO, which are unique to CLL among all other B cell malignancies, but they are observed in inflamed tissues of patients with systemic autoimmune disorders as well (1). Functional similarities between inflammation- and CLL-associated PC may include their capacity to initiate or maintain autoantigen-stimulation, indicating that autoimmune diseases and CLL could share part of their pathogenic trait. The occurrence of FDCs in PCs has been reported (58), thus supporting the view that leukemia B cell-FDC encounter is a major source of cellular proliferation.

We infer from our data that leukemia cell-associated LTαβ confers the required ligand such that FDC-networks can be induced *de novo*. In this paracrine network, further FDC stimulation with cell-bound LTαβ can induce the expression of CXCL13 and other pro-inflammatory cytokines (59). To break this feedback-loop, we treated mice with an LTβR-Ig fusion protein and found that targeting the LTβR signaling pathway profoundly retarded murine CLL growth. FDC loss and CXCL13 reduction indicated that inhibition of stroma-lymphoma cell crosstalk can translate into an ameliorated clinical course. Targeting the stromal environment in SLOs is an appealing treatment option for indolent lymphoma because these benign compartments are subject to low selective pressure for mutations and epigenetic changes (60).

We propose that our stroma induction model can mimic an early pathogenic condition where, upon arrival of transformed clonal CLL cells in SLO, leukemia cells encounter a microenvironment that enhances their proliferation. Reciprocally, tumor cells impose stroma remodeling. Increased proliferative activity in proximity to FDC networks could enhance genetic vulnerability, resulting in mutation acquisitions that render tumor cells increasingly independent from antigenic triggering (1).

When applying an LTβR-decoy receptor, selective targeting of the stroma interface alone led to tumor growth retardation; this strategy is applicable to a minimal residual disease state where tumor cells might be protected in LT-dependent niches. Furthermore, it may be possible to inhibit leukemia cell access to antigen-presenting cells, either through selective interference with CXCR5 activity as shown here, or by targeting the FDC function in growth factor supply. Both immunological treatments are rational strategies to complement traditional cytotoxic therapies for the cure of leukemia and lymphoma.

Methods

More detailed methods can be found in the Supplemental Methods.

Microarray data

The Microarray data presented in this publication have been deposited in NCBI's Gene Expression Omnibus (61) and are accessible through GEO Series accession number GSE60925.

Chemotaxis assay

Assays were performed in 5-μm-pore transwell plates (Corning) for 4 hr at 37°C, exactly as described (16). CCL21, CXCL12 and CXCL13 were used at a concentration of 100 nM, 25 nM and 300 nM, respectively (R&D Research Diagnostics).

Patient CLL blood samples

Peripheral blood samples from treatment naïve CLL patients were purified over a Ficoll gradient. Tumor cells ($CD19^+CD5^+$) were FACS-sorted and RNA was immediately extracted. The study was conducted according to the declaration of Helsinki and in accordance with local ethical guidelines; written informed consent of all patients was obtained.

Generation of primary *Eμ-Tcl1* leukemia cells for transplantation

Eμ-Tcl1 transgenic mice were monitored for signs of disease by quantification of the frequency of tumor cells in PB by flow cytometry ($CD5^+CD19^+$). Spleen-derived leukemia cell suspensions were prepared from diseased mice (> 8 months old and tumor

cell load > 50% in the periphery) by tissue homogenization, depletion of red blood cells and FACS-sorting.

Cell lines

Murine bone marrow stromal cells (M2-10B4; ATCC-CRL-1972) were obtained from ATCC in July 2010. The cells were passaged 2-3 times over a period of three weeks and aliquots were frozen in liquid nitrogen. All experiments were performed with these aliquots. The human follicular dendritic cell line FDC/HK was obtained from Y. S. Choi (Ochner Clinic foundation New Orleans, LA, USA) in 2011 and cultured as described above. No further authentication was done for both cell lines.

***In vivo* blockade of the LTβ-receptor signalling pathway**

100 µg of blocking LtβR-Ig (murine receptor fused to mouse mAb IgG1; Biogen Idec or generated as described (62) or isotype control antibody (MOPC 21) were injected repeatedly i.p. into tumor challenged and *Eμ-Tcl1* transgenic mice, respectively.

Statistical analysis

Results are expressed as arithmetic means ± SEM if not otherwise indicated. Values of $P \leq 0.05$ were considered statistically significant, as determined by the unpaired Mann-Whitney test, the 2-tailed unpaired Student's *t* test, or the Wilcoxon signed rank test where appropriate.

Author's Contribution

Conception and design: U.E. Höpken, A. Rehm

Development of methodology: K. Heinig, M. Gätjen, M. Grau, V. Stache, A. Rehm, U.E. Höpken

Acquisition of data (provided reagents and animals): I. Anagnostopoulos, T. Hehlgans, R. Brink, J. Westermann

Analysis and interpretation of data: K. Heinig, M. Gätjen, M. Grau, K. Gerlach, V. Stache, R.A. Niesner, Z. Cseresnyes, A.E. Hauser, P. Lenz, G. Lenz, A. Rehm, U.E. Höpken

Administrative, technical, or material support: B. Dörken, M. Lipp

Writing the manuscript: U.E. Höpken, K. Heinig, A. Rehm

All authors reviewed the manuscript

Study supervision: U.E. Höpken, A. Rehm

Acknowledgments

We thank Carlo Croce (Columbus University, OH, USA) and Jeffrey L. Browning (Biogen Idec, Cambridge, MA, USA) for providing us with essential reagents and Heike Schwede and Kerstin Krüger for excellent technical assistance.

Grant Support

This work was funded by grants from the Deutsche Krebshilfe (grant number 107749), German Research Foundation (DFG), and the Berliner Krebsgesellschaft to U.E.H. and A.R., grants from the DFG, the Deutsche Krebshilfe and the Else Kröner-Fresenius-Stiftung to G.L., DFG-funded project "JIMI-a network for intravital microscopy" to R.N., Z.C. and A.E.H., and by a Doctoral Scholarship from the Philipps-Universität Marburg to M.G.

References

1. Caligaris-Cappio F. Inflammation, the microenvironment and chronic lymphocytic leukemia. Haematologica. 2011 Mar;96(3):353-5. PubMed PMID: 21357715. Epub 2011/03/02. eng.
2. Munk Pedersen I, Reed J. Microenvironmental interactions and survival of CLL B-cells. Leuk Lymphoma. 2004 Dec;45(12):2365-72. PubMed PMID: 15621749. Epub 2004/12/29. eng.
3. Zenz T, Mertens D, Kuppers R, Dohner H, Stilgenbauer S. From pathogenesis to treatment of chronic lymphocytic leukaemia. Nat Rev Cancer. 2010 Jan;10(1):37-50. PubMed PMID: 19956173. Epub 2009/12/04. eng.
4. Ishibe N, Sgambati MT, Fontaine L, Goldin LR, Jain N, Weissman N, et al. Clinical characteristics of familial B-CLL in the National Cancer Institute Familial Registry. Leuk Lymphoma. 2001 Jun;42(1-2):99-108. PubMed PMID: 11699227. Epub 2001/11/09. eng.
5. Küppers R. Mechanisms of B-cell lymphoma pathogenesis. Nat Rev Cancer. 2005 Apr;5(4):251-62. PubMed PMID: 15803153. Epub 2005/04/02. eng.
6. Seifert M, Sellmann L, Bloehdorn J, Wein F, Stilgenbauer S, Durig J, et al. Cellular origin and pathophysiology of chronic lymphocytic leukemia. J Exp Med. 2012 Oct 22. PubMed PMID: 23091163. Epub 2012/10/24. Eng.
7. Klein U, Tu Y, Stolovitzky GA, Mattioli M, Cattoretti G, Husson H, et al. Gene expression profiling of B cell chronic lymphocytic leukemia reveals a homogeneous phenotype related to memory B cells. J Exp Med. 2001 Dec 3;194(11):1625-38. PubMed PMID: 11733577. Epub 2001/12/26. eng.
8. Rosenwald A, Alizadeh AA, Widhopf G, Simon R, Davis RE, Yu X, et al. Relation of gene expression phenotype to immunoglobulin mutation genotype in B cell chronic lymphocytic leukemia. J Exp Med. 2001 Dec 3;194(11):1639-47. PubMed PMID: 11733578. Epub 2001/12/26. eng.
9. Chiorazzi N, Ferrarini M. Cellular origin(s) of chronic lymphocytic leukemia: cautionary notes and additional considerations and possibilities. Blood. 2011 Feb 10;117(6):1781-91. PubMed PMID: 21148333. Epub 2010/12/15. eng.
10. Kikushige Y, Ishikawa F, Miyamoto T, Shima T, Urata S, Yoshimoto G, et al. Self-renewing hematopoietic stem cell is the primary target in pathogenesis of human chronic lymphocytic leukemia. Cancer Cell. 2011 Aug 16;20(2):246-59. PubMed PMID: 21840488. Epub 2011/08/16. eng.
11. Dohner H, Stilgenbauer S, Benner A, Leupolt E, Krober A, Bullinger L, et al. Genomic aberrations and survival in chronic lymphocytic leukemia. N Engl J Med. 2000 Dec 28;343(26):1910-6. PubMed PMID: 11136261. Epub 2001/01/03. eng.
12. Herling M, Patel KA, Weit N, Lilienthal N, Hallek M, Keating MJ, et al. High TCL1 levels are a marker of B-cell receptor pathway responsiveness and adverse outcome in chronic lymphocytic leukemia. Blood. 2009 Nov 19;114(21):4675-86. PubMed PMID: 19770358. Epub 2009/09/23. eng.
13. Bichi R, Shinton SA, Martin ES, Koval A, Calin GA, Cesari R, et al. Human chronic lymphocytic leukemia modeled in mouse by targeted TCL1 expression. Proc Natl Acad Sci U S A. 2002 May 14;99(10):6955-60. PubMed PMID: 12011454. Epub 2002/05/16. eng.
14. Pals ST, de Gorter DJ, Spaargaren M. Lymphoma dissemination: the other face of lymphocyte homing. Blood. 2007 Nov 1;110(9):3102-11. PubMed PMID: 17656647. Epub 2007/07/28. eng.

15. Burger JA, Kipps TJ. Chemokine receptors and stromal cells in the homing and homeostasis of chronic lymphocytic leukemia B cells. Leuk Lymphoma. 2002 Mar;43(3):461-6. PubMed PMID: 12002747. Epub 2002/05/11. eng.
16. Höpken UE, Foss HD, Meyer D, Hinz M, Leder K, Stein H, et al. Up-regulation of the chemokine receptor CCR7 in classical but not in lymphocyte-predominant Hodgkin disease correlates with distinct dissemination of neoplastic cells in lymphoid organs. Blood. 2002 Feb 15;99(4):1109-16. PubMed PMID: 11830455. Epub 2002/02/07. eng.
17. Höpken UE, Rehm A. Homeostatic chemokines guide lymphoma cells to tumor growth-promoting niches within secondary lymphoid organs. J Mol Med 2012 (Berl). Nov;90(11):1237-45. PubMed PMID: 22577036. Epub 2012/05/12. eng.
18. Gine E, Martinez A, Villamor N, Lopez-Guillermo A, Camos M, Martinez D, et al. Expanded and highly active proliferation centers identify a histological subtype of chronic lymphocytic leukemia ("accelerated" chronic lymphocytic leukemia) with aggressive clinical behavior. Haematologica. 2010 Sep;95(9):1526-33. PubMed PMID: 20421272. Epub 2010/04/28. eng.
19. Liberzon A, Subramanian A, Pinchback R, Thorvaldsdottir H, Tamayo P, Mesirov JP. Molecular signatures database (MSigDB) 3.0. Bioinformatics. 2011 Jun 15;27(12):1739-40. PubMed PMID: 21546393. Epub 2011/05/07. eng.
20. Kanehisa M, Goto S, Sato Y, Furumichi M, Tanabe M. KEGG for integration and interpretation of large-scale molecular data sets. Nucleic Acids Res. 2012 Jan;40(Database issue):D109-14. PubMed PMID: 22080510. Epub 2011/11/15. eng.
21. Yan XJ, Albesiano E, Zanesi N, Yancopoulos S, Sawyer A, Romano E, et al. B cell receptors in TCL1 transgenic mice resemble those of aggressive, treatment-resistant human chronic lymphocytic leukemia. Proc Natl Acad Sci U S A. 2006 Aug 1;103(31):11713-8. PubMed PMID: 16864779. Epub 2006/07/26. eng.
22. Rehm A, Mensen A, Schradi K, Gerlach K, Wittstock S, Winter S, et al. Cooperative function of CCR7 and lymphotoxin in the formation of a lymphoma-permissive niche within murine secondary lymphoid organs. Blood. 2011 Jul 28;118(4):1020-33. PubMed PMID: 21586747. Epub 2011/05/19. eng.
23. Seke Etet PF, Vecchio L, Nwabo Kamdje AH. Interactions between bone marrow stromal microenvironment and B-chronic lymphocytic leukemia cells: any role for Notch, Wnt and Hh signaling pathways? Cell Signal. 2012 Jul;24(7):1433-43. PubMed PMID: 22446006. Epub 2012/03/27. eng.
24. Komori T. Regulation of bone development and maintenance by Runx2. Front Biosci. 2008;13:898-903. PubMed PMID: 17981598. Epub 2007/11/06. eng.
25. Bajenoff M, Egen JG, Koo LY, Laugier JP, Brau F, Glaichenhaus N, et al. Stromal cell networks regulate lymphocyte entry, migration, and territoriality in lymph nodes. Immunity. 2006 Dec;25(6):989-1001. PubMed PMID: 17112751. Epub 2006/11/23. eng.
26. Cinamon G, Zachariah MA, Lam OM, Foss FW, Jr., Cyster JG. Follicular shuttling of marginal zone B cells facilitates antigen transport. Nat Immunol. 2008 Jan;9(1):54-62. PubMed PMID: 18037889. Epub 2007/11/27. eng.
27. Gatto D, Brink R. B cell localization: regulation by EBI2 and its oxysterol ligand. Trends Immunol. 2013 Jul;34(7):336-41. PubMed PMID: 23481574. Epub 2013/03/14. eng.
28. Chen L, Widhopf G, Huynh L, Rassenti L, Rai KR, Weiss A, et al. Expression of ZAP-70 is associated with increased B-cell receptor signaling in chronic lymphocytic leukemia. Blood. 2002 Dec 15;100(13):4609-14. PubMed PMID: 12393534. Epub 2002/10/24. eng.

29. Herman SE, Gordon AL, Hertlein E, Ramanunni A, Zhang X, Jaglowski S, et al. Bruton tyrosine kinase represents a promising therapeutic target for treatment of chronic lymphocytic leukemia and is effectively targeted by PCI-32765. Blood. 2011 Jun 9;117(23):6287-96. PubMed PMID: 21422473. Pubmed Central PMCID: 3122947.
30. Woyach JA, Bojnik E, Ruppert AS, Stefanovski MR, Goettl VM, Smucker KA, et al. Bruton's tyrosine kinase (BTK) function is important to the development and expansion of chronic lymphocytic leukemia (CLL). Blood. 2014 Feb 20;123(8):1207-13. PubMed PMID: 24311722. Pubmed Central PMCID: 3931190.
31. Woyach JA, Furman RR, Liu TM, Ozer HG, Zapatka M, Ruppert AS, et al. Resistance mechanisms for the Bruton's tyrosine kinase inhibitor ibrutinib. N Engl J Med. 2014 Jun 12;370(24):2286-94. PubMed PMID: 24869598.
32. Gobessi S, Laurenti L, Longo PG, Sica S, Leone G, Efremov DG. ZAP-70 enhances B-cell-receptor signaling despite absent or inefficient tyrosine kinase activation in chronic lymphocytic leukemia and lymphoma B cells. Blood. 2007 Mar 1;109(5):2032-9. PubMed PMID: 17038529. Epub 2006/10/14. eng.
33. Kim HS, Zhang X, Klyushnenkova E, Choi YS. Stimulation of germinal center B lymphocyte proliferation by an FDC-like cell line, HK. J Immunol. 1995 Aug 1;155(3):1101-9. PubMed PMID: 7543513. Epub 1995/08/01. eng.
34. Mourcin F, Pangault C, Amin-Ali R, Ame-Thomas P, Tarte K. Stromal cell contribution to human follicular lymphoma pathogenesis. Front Immunol. 2012 3:280. PubMed PMID: 22973275. Epub 2012/09/14. eng.
35. El Shikh ME, Pitzalis C. Follicular dendritic cells in health and disease. Front Immunol. 2012 3:292. PubMed PMID: 23049531. Epub 2012/10/11. eng.
36. Allen CD, Ansel KM, Low C, Lesley R, Tamamura H, Fujii N, et al. Germinal center dark and light zone organization is mediated by CXCR4 and CXCR5. Nat Immunol. 2004 Sep;5(9):943-52. PubMed PMID: 15300245. Epub 2004/08/10. eng.
37. Green JA, Suzuki K, Cho B, Willison LD, Palmer D, Allen CD, et al. The sphingosine 1-phosphate receptor S1P(2) maintains the homeostasis of germinal center B cells and promotes niche confinement. Nat Immunol. 2011 Jul;12(7):672-80. PubMed PMID: 21642988. Epub 2011/06/07. eng.
38. Roozendaal R, Mebius RE. Stromal cell-immune cell interactions. Annu Rev Immunol. 2011 Apr 23;29:23-43. PubMed PMID: 21073333. Epub 2010/11/16. eng.
39. Burger JA. Chemokines and chemokine receptors in chronic lymphocytic leukemia (CLL): from understanding the basics towards therapeutic targeting. Semin Cancer Biol. 2010 Dec;20(6):424-30. PubMed PMID: 20883788.
40. Burger JA, Burger M, Kipps TJ. Chronic lymphocytic leukemia B cells express functional CXCR4 chemokine receptors that mediate spontaneous migration beneath bone marrow stromal cells. Blood. 1999 Dec 1;94(11):3658-67. PubMed PMID: 10572077. Epub 1999/11/26. eng.
41. Burkle A, Niedermeier M, Schmitt-Graff A, Wierda WG, Keating MJ, Burger JA. Overexpression of the CXCR5 chemokine receptor, and its ligand, CXCL13 in B-cell chronic lymphocytic leukemia. Blood. 2007 Nov 1;110(9):3316-25. PubMed PMID: 17652619. Epub 2007/07/27. eng.
42. Messmer BT, Messmer D, Allen SL, Kolitz JE, Kudalkar P, Cesar D, et al. In vivo measurements document the dynamic cellular kinetics of chronic lymphocytic leukemia B cells. J Clin Invest. 2005 Mar;115(3):755-64. PubMed PMID: 15711642. Epub 2005/02/16. eng.
43. Herishanu Y, Perez-Galan P, Liu D, Biancotto A, Pittaluga S, Vire B, et al. The lymph node microenvironment promotes B-cell receptor signaling, NF-kappaB

activation, and tumor proliferation in chronic lymphocytic leukemia. Blood. 2011 Jan 13;117(2):563-74. PubMed PMID: 20940416. Epub 2010/10/14. eng.
44. Forster R, Mattis AE, Kremmer E, Wolf E, Brem G, Lipp M. A putative chemokine receptor, BLR1, directs B cell migration to defined lymphoid organs and specific anatomic compartments of the spleen. Cell. 1996 Dec 13;87(6):1037-47. PubMed PMID: 8978608. Epub 1996/12/13. eng.
45. Höpken UE, Achtman AH, Kruger K, Lipp M. Distinct and overlapping roles of CXCR5 and CCR7 in B-1 cell homing and early immunity against bacterial pathogens. J Leukoc Biol. 2004 Sep;76(3):709-18. PubMed PMID: 15197239. Epub 2004/06/16. eng.
46. Bajenoff M, Glaichenhaus N, Germain RN. Fibroblastic reticular cells guide T lymphocyte entry into and migration within the splenic T cell zone. J Immunol. 2008 Sep 15;181(6):3947-54. PubMed PMID: 18768849. Epub 2008/09/05. eng.
47. Pekarsky Y, Calin GA, Aqeilan R. Chronic lymphocytic leukemia: molecular genetics and animal models. Curr Top Microbiol Immunol. 2005;294:51-70. PubMed PMID: 16323427. Epub 2005/12/06. eng.
48. Pillai S, Cariappa A. The follicular versus marginal zone B lymphocyte cell fate decision. Nat Rev Immunol. 2009 Nov;9(11):767-77. PubMed PMID: 19855403. Epub 2009/10/27. eng.
49. Martin F, Kearney JF. B1 cells: similarities and differences with other B cell subsets. Curr Opin Immunol. 2001 Apr;13(2):195-201. PubMed PMID: 11228413. Epub 2001/03/03. eng.
50. Wen L, Shinton SA, Hardy RR, Hayakawa K. Association of B-1 B cells with follicular dendritic cells in spleen. J Immunol. 2005 Jun 1;174(11):6918-26. PubMed PMID: 15905534. Epub 2005/05/21. eng.
51. Saez de Guinoa J, Barrio L, Mellado M, Carrasco YR. CXCL13/CXCR5 signaling enhances BCR-triggered B-cell activation by shaping cell dynamics. Blood. 2011 Aug 11;118(6):1560-9. PubMed PMID: 21659539. Epub 2011/06/11. eng.
52. Fais F, Ghiotto F, Hashimoto S, Sellars B, Valetto A, Allen SL, et al. Chronic lymphocytic leukemia B cells express restricted sets of mutated and unmutated antigen receptors. J Clin Invest. 1998 Oct 15;102(8):1515-25. PubMed PMID: 9788964. Epub 1998/10/28. eng.
53. Duhren-von Minden M, Ubelhart R, Schneider D, Wossning T, Bach MP, Buchner M, et al. Chronic lymphocytic leukaemia is driven by antigen-independent cell-autonomous signalling. Nature. 2012 Sep 13;489(7415):309-12. PubMed PMID: 22885698. Epub 2012/08/14. eng.
54. Greaves M. Clonal expansion in B-CLL: fungal drivers or self-service? J Exp Med. 2013 Jan 14;210(1):1-3. PubMed PMID: 23319726. Pubmed Central PMCID: 3549708.
55. Fu YX, Huang G, Wang Y, Chaplin DD. B lymphocytes induce the formation of follicular dendritic cell clusters in a lymphotoxin alpha-dependent fashion. J Exp Med. 1998 Apr 6;187(7):1009-18. PubMed PMID: 9529317. Epub 1998/05/16. eng.
56. Tumanov A, Kuprash D, Lagarkova M, Grivennikov S, Abe K, Shakhov A, et al. Distinct role of surface lymphotoxin expressed by B cells in the organization of secondary lymphoid tissues. Immunity. 2002 Sep;17(3):239-50. PubMed PMID: 12354378. Epub 2002/10/02. eng.
57. Gonzalez M, Mackay F, Browning JL, Kosco-Vilbois MH, Noelle RJ. The sequential role of lymphotoxin and B cells in the development of splenic follicles. J Exp Med. 1998 Apr 6;187(7):997-1007. PubMed PMID: 9529316. Epub 1998/05/16. eng.

58. Schmid C, Isaacson PG. Proliferation centres in B-cell malignant lymphoma, lymphocytic (B-CLL): an immunophenotypic study. Histopathology. 1994 May;24(5):445-51. PubMed PMID: 8088716. Epub 1994/05/01. eng.
59. Ansel KM, Ngo VN, Hyman PL, Luther SA, Forster R, Sedgwick JD, et al. A chemokine-driven positive feedback loop organizes lymphoid follicles. Nature. 2000 Jul 20;406(6793):309-14. PubMed PMID: 10917533. Epub 2000/08/05. eng.
60. Acharyya S, Oskarsson T, Vanharanta S, Malladi S, Kim J, Morris PG, et al. A CXCL1 paracrine network links cancer chemoresistance and metastasis. Cell. 2012 Jul 6;150(1):165-78. PubMed PMID: 22770218. Epub 2012/07/10. eng.
61. Edgar R, Domrachev M, Lash AE. Gene Expression Omnibus: NCBI gene expression and hybridization array data repository. Nucleic Acids Res. 2002 Jan 1;30(1):207-10. PubMed PMID: 11752295. Pubmed Central PMCID: 99122.
62. Stopfer P, Obermeier F, Dunger N, Falk W, Farkas S, Janotta M, et al. Blocking lymphotoxin-beta receptor activation diminishes inflammation via reduced mucosal addressin cell adhesion molecule-1 (MAdCAM-1) expression and leucocyte margination in chronic DSS-induced colitis. Clin Exp Immunol. 2004 Apr;136(1):21-9. PubMed PMID: 15030510. Epub 2004/03/20. eng.

Figure Legends

Figure 1. CXCR5 expression accelerates *Eμ-Tcl1* leukemogenesis and is indispensable for tumor cell recruitment to lymphoid B cell follicles. (**A**) Tumor load in spleen, LN, PB, and BM of 7-19 (n=12-19), 20-27 (n=8-17), 28-39 (n=36-52), and 40-48 (n=12-52) week-old *Eμ-Tcl1* and 7-19 (n=9-15), 20-27 (n=10-12), 28-39 (n=9-42), and 40-48 (n=16-20) week-old *Cxcr5*$^{-/-}$*Eμ-Tcl1* mice. CD19^{+}B220^{low}CD5^{+} tumor cells are presented as percentages of all lymphocytes with means. Error bars indicate Min to Max. P values were determined by unpaired Student's *t* test. (**B**) Chemokine receptor expression on splenic CD19^{+}B220^{low}CD5^{+} gated tumor cells of diseased *Eμ-Tcl1* and *Cxcr5*$^{-/-}$*Eμ-Tcl1* mice (n=4-7 mice per marker; isotype control; shaded curve). (**C**) Chemotaxis of *Eμ-Tcl1* (left panel) or *Cxcr5*$^{-/-}$*Eμ-Tcl1* (right panel) cells towards CCL21 (100 nM), CXCL12 (25 nM), and CXCL13 (300 nM). Error bars indicate mean ± SEM of three independent experiments with triplicates for each chemokine. P values were determined by Mann-Whitney test. (**D**) Adoptive transfer of 2 x 10^{7} splenic leukemia cells of *Eμ-Tcl1* and *Cxcr5*$^{-/-}$*Eμ-Tcl1* mice (CD45.2^{+}) into CD45.1^{+} B6 recipients. Three days after i.v. transfer, spleen sections were stained for CD45.2^{+} tumor cells, CD3^{+} T cells, and IgD^{+} B cells (n=8-9 per group; upper part). Lower panel, detection of tumor cells, B cells, and MOMA-1^{+} metallophilic macrophages (n=8-9 per group). Scale bars, 100 μm. (**E**) *In vivo* blockage of the CXCL13 signaling pathway by treatment of tumor challenged mice (1 x 10^{6} *Eμ-Tcl1* cells i.v. on day 1) with 50 μg anti-CXCL13 or isotype Ab i.p. at the days indicated (n=3 per group). Tumor cell (CD19^{+}B220^{low}CD5^{+}) load was assessed by flow cytometry at day 24. Error bars indicate mean ± SEM. P values were determined by unpaired Student's *t* test. *P ≤ 0.05, **P ≤ 0.01, *P ≤ 0.05, ***P ≤ 0.001.

Figure 2. Differential gene expression signatures of *Eμ-Tcl1* and CXCR5-deficient *Eμ-Tcl1* leukemia cells. (**A**) Gene expression profiling of sorted *Eμ-Tcl1* (n=6) or *Cxcr5*$^{-/-}$*Eμ-Tcl1* (n=5) leukemia cells. Human genes in the signature definition without a homolog mouse gene and genes without measurement data are depicted in grey. Gene expression profiles were analysed by GSEA. A representative proliferation signature is shown (Molecular Signature DB v3.1; GNF2 CDC2 cancer gene neighbourhood). Gene expression levels are shown relative to the mean of all animals and were averaged over all animals of each genotype. The signature average for each genotype is depicted at the bottom (paired Student's t-tests against zero regulation; error bars indicate SEMs). (**B)** Enrichment plot of the proliferation signature shown in (**A**). Blue lines mark genes in the signature; the p value of the enrichment score (permutation test), and the false discovery rate (relative to the cancer gene neighbourhoods sub-category of the Molecular Signature Database v3.1) are indicated. **(C)** Gene expression profiles of *Eμ-Tcl1*- versus *Cxcr5*$^{-/-}$ *Eμ-Tcl1*-derived tumor cells were analyzed by GSEA, as in (**A**). In 83 out of 84 gene signatures related to apoptosis a differential regulation between *Eμ-Tcl1* and *Cxcr5*$^{-/-}$*Eμ-Tcl1* animals was not found. Relative expression for all genes belonging to the representative KEGG apoptosis pathway are shown here. The average signature expression determined by paired Student's t-tests against zero regulation; error bars indicate SEMs. (**D, E**) B-1 and MZ B cells were compared and the top 100 down- (**D**) and up- (**E**) regulated genes were identified. Shown are relative gene expression levels of these genes in *Eμ-Tcl1* tumor cells versus Wt total follicular cells. Genes found upregulated in B-1 versus MZ B cells were also found upregulated in Eμ- *Tcl1* tumor versus Wt total follicular cells and likewise for downregulated genes. (**F**) Proliferation of *Eμ-Tcl1* or *Cxcr5*$^{-/-}$*Eμ-Tcl1* leukemia cells cocultured with or without a M2-10B4

stromal layer was analyzed by an enzymatic activity assay (Cell Titer 96 AQ_{eous} One Solution Cell Proliferation Assay from Promega) measuring the absorbance of a formazan product after 48 hours. The quantity of the formazan product as measured by the absorbance at 450-540 nm is directly proportional to the number of living cells in the culture. Bars indicate mean ± SEM of three independent experiments; P value was determined by unpaired Student's *t* test.

Figure 3. *Eμ-Tcl1* tumor cells exhibit different migratory routes and temporal migration pattern to and within lymphoid follicles compared to B lymphocytes. (A and **B)** 2 x 10^7 SNARF-1 labeled (red) splenic *Eμ-Tcl1* leukemia cells or follicular B cells were transferred i.v. into B6 mice. Spleen sections were stained for MOMA-1^+ metallophillic macrophages and $B220^+$ B cells to distinguish the MZ (MOMA-1^+B220^+; MZ), the B cell follicle (MOMA-1^-B220^+; Fo), red pulp (RP) and T cell zone (MOMA-1^- B220; T) and one representative section is shown for each time point. Scale bar, 100 μm. **(C)** Quantification of Wt B cells and *Eμ-Tcl1* leukemia cell localization within the zones as indicated in **(A** and **B)**. **(D)** The percentage of B cells or Eμ-*Tcl1* leukemia cells located at the B/T cell border or in the $MOMA^-B220^+$ B cell zone is presented as a time curve. Bars represent mean ± SEM of two independent experiments with n=2-5 mice for each group and time point. P values were determined by unpaired Student's *t* test. *P ≤ 0.05, **P ≤ 0.01; n.s., non significant.

Figure 4. Functional interaction of *Eμ-Tcl1* tumor cells with FDC networks.

(A) Splenic *Eμ-Tcl1* leukemia cells were sorted and 2x10^7 SNARF-1 labeled cells (red) were transferred i.v. into recipient mice (n=3). Eight hrs later, spleen sections were stained for $CD21^+CD35^+$ FDCs and $B220^+$ B cells. A zoomed inlet (boxed area; left

panel) is aditionally shown. Scale bar, 100 μm. (**B**) 2x10^7 *Eμ-Tcl1* leukemia cells were transferred i.v. into congenic recipient mice. Three days later spleen sections were stained for tumor cells (CD45.2$^+$), FDC-M2$^+$ FDCs, and the proliferation marker Ki67 (6-9 sections per mouse; n=3). **(C)** Splenic follicular B cells (B220$^+$CD21^{int}CD23^{hi}) and *Eμ-Tcl1* lymphoma cells were sorted and labeled with CMAC (FoB, in blue) and SNARF-1 (leukemia cells, in red), respectively. 1x10^7 cells of both groups were co-transferred into recipient mice (n=3) and localization was analyzed after 8 hrs. A representative section and an enlarged inlet of the boxed area are shown. Scale bar, 50 μm. (**D**) Quantification of the proportion of transferred leukemia cells compared to follicular B cells localized within the FDC rich zone of the B cell follicle, as marked by the dashed white line in (**C**). Error bars indicate mean ± SEM of three independent experiments with a total of 9-13 analyzed sections. (**E)** Immunoblot analysis of phosphorylated ZAP-70/Syk from leukemia cells (n=14 mice; #1 and #2 indicate two representative leukemia samples), and follicular B cells (n=4 mice, one representative sample depicted) as a control. Membranes were incubated with anti-phospho-ZAP-70^{Tyr319}/Syk^{Tyr352} (top panel), and anti-Gapdh (bottom panel). Bar diagram depicts the quantification of the ratios. Error bars indicate mean ± SEM. (F) Immunoblot analysis of phosphorylated and total BTK from leukemia cells (n=3 mice; #1-3 indicate three leukemia samples), and follicular B cells (n=3 mice, #1-3; three samples) as a control. Membranes were incubated with anti-p-BTK (top panel), and total BTK (bottom panel). Bar diagram depicts the quantification of the ratios. Error bars indicate mean ± SEM. (**G**) *Eμ-Tcl1* mice with a tumor burden of 21-25% (n=10) in PB were injected i.p. with 1 mg BrdU for three days. PB, spleen, and peritoneal cavity (PerC)-derived Eμ-*Tcl1* leukemia cells were analyzed for BrdU uptake. (**H, I**) One x10^5 splenic-derived *Eμ-Tcl1* leukemia cells were seeded in triplicates on top of unstimulated (control group) or LTα1β2

prestimulated FDC-HK stroma cells alone, or together with cytokines, growth factors, the CXCR4 antagonist AMD3100 or the Notch-inhibitor DAPT, as indicated. After 72 hrs, viable leukemia cells were counted (**H**). In (**I**) after 24 and 48 hrs, cultures were supplemented with 10 µM BrdU and BrdU uptake was analyzed by flow cytometry 72 hrs thereafter. Results are shown as x-fold cell proliferation relative to control (FDC-HK + *Eμ-Tcl1* leukemia B cells), set arbitrarily to 1 (indicated by a horizontal line; n=7 (H), separate *Eμ-Tcl1* cell clones tested). Error bars indicate mean ± SEM of 5-7 independent experiments. P values were determined by Mann-Whitney test. Tracks of motile *Eμ-Tcl1* leukemia cells (**J;** upper panel) or motile B lymphocytes (**J;** lower panel) that are localized within the B cell follicle at the FDCs, visualized by staining with AF568-labeled anti-$CD21^+CD35^+$ Fab fragments (red), are projected onto an image of the entire z stack representing a midpoint in the imaging time period of a representative experiment from 2 independent experiments (n=4 mice per group). **(K)** Quantitation of displacement rate, (**L**) track velocity, and (**M**) track length of follicle (Fo)- or FDC-located B cells and *Eμ-Tcl1* lymphoma cells. Means and significances calculated by the unpaired Student's *t* test are shown. *P ≤ 0.05; **P ≤ 0.01; ***P ≤ 0.001; n.s., non significant.

Figure 5. *Eμ-Tcl1* tumor cell localize in the GC-associated FDC rich light zone independently of *Cxcr4* and *S1pr2* signaling. (A) Wt mice were immunized with SRBCs. At day 7, $2x10^7$ SNARF-1 labeled sorted splenic *Eμ-Tcl1* tumor cells were transferred i.v. into recipients. Eight hrs later, localization of tumor cells (red) was detected in splenic sections by staining for GC-associated FDC rich light zone ($CD21^+CD35^+$) and PNA^+ dark zone (left panel) or by staining of IgD^+ B cell follicular areas and PNA^+ dark zone (right panel). Two consecutive slides were stained. Scale bar, 50 µm. **(B)** B6 mice were immunized as in (**A**). At day 8, $2x10^7$ sorted splenic *Eμ-Tcl1*

leukemia cells were pre-treated without (2 independent experiments) or with AMD3100 (3 independent experiments), followed by i.v. transfer into recipient mice. Eight hrs later, localization of tumor cells (red) was detected in splenic sections by staining for GC-associated FDC rich light zone ($CD21^+CD35^+$) and PNA^+ dark zone (upper panel) and for $CD21^+CD35^+$ FDCs and $B220^+$ B cells (lower panel). (**C**) Quantification of the proportion of leukemia cells within the light zone (green) or within the PNA^+ dark zone (blue). Bars represent mean ± SEM of 3-5 independent experiments. **(D)** Chemotaxis of *Eμ-Tcl1* tumor cells toward CXCL12 with and without treatment with AMD3100. Bars represent mean ± SEM of 2-4 independent experiments with triplicates per each group. P values were determined by a Mann-Whitney test. *$P \leq 0.05$; ***$P \leq 0.001$. **(E)** Quantitative RT-PCR of *S1pr2* in sorted tumor cells of *Eμ-Tcl1* (n=4) mice, and in follicular B ($B220^+CD21^{lo}CD23^{hi}$; Fo B), marginal zone B ($B220^+CD21^{hi}CD23^{lo}$; MZ B) and germinal center B ($B220^+GL7^+Fas^+$; GC B) cells (one experiment with three mice per group). Transcript expression was normalized to Gapdh. Error bars indicate mean ± SEM.

Figure 6. *Eμ-Tcl1* tumor cells localize at radio-resistant FDC networks and exhibit stronger proliferation in the spleens of irradiated mice. (**A**) Spleens of lethally irradiated (9.25 Gy) or untreated B6 CD45.1 mice were harvested 48 hrs (n=2 per group) after treatment and stained for $B220^+$ B cells, MAdCAM-1^+ MRCs and FDC-$M2^+$ stromal cell networks. Representative sections are shown (upper panels). 2 x 10^7 SNARF-labeled *Eμ-Tcl1* cells (CD45.2) were adoptively transferred into lethally irradiated recipients (n=3) or into non-irradiated controls (n=2). 48 hrs after tumor challenge spleen sections were stained with $CD45.2^+$ and FDC-$M2^+$ (blue) (lower panels) or (**B**), $CD45.2^+$, FDC-$M2^+$, and Ki-67^+ antibodies. Representative sections are shown.

Scale bars, 100 μm. (**C**) 2-5 x 10^6 eFluor670-labeled *Eμ-Tcl1* leukemia cells were adoptively transferred into irradiated mice (n=3) or into untreated recipients (n=2). 48 hrs later, proliferation of splenic tumor cells was evaluated according to eFluor670 dilution; a representative histogram shows staining of tumor cells recovered from untreated or irradiated mice. (**D**) Splenic BAFF and APRIL mRNA transcripts of irradiated or non-irradiated mice with or without tumor cell challenge (n=2-3 mice per group). Transcript expression was normalized to Gapdh. Error bars indicate mean ± SEM. (**E**) Surface expression of BAFFR on splenic *Eμ-Tcl1* leukemia cells ($CD19^+CD5^+$; n=5 transgenic *Eμ-Tcl1* mice) was confirmed by flow cytometry (isotype Ig control, shaded curve; anti-BAFFR Ig, solid line). (**F**) Blockage of the BAFF signaling pathway by injecting 50 μg anti-BAFF or isotype Ab together with 5-10 x 10^6 eFluor670-labeled *Eμ-Tcl1* leukemia cells i.v. (n=3-4 per group). 48 hrs later, proliferation of splenic tumor cells was evaluated according to eFluor670 dilution; a representative histogram shows staining of tumor cells recovered from isotype or anti-BAFF treated irradiated mice (left panel). Relative proportion of proliferated leukemia cells from isotype and anti-BAFF treated irradiated mice compared to cells from non-irradiated mice (set arbitrarily to 100%; n=3 independent experiments) are depicted as bars ± SEM (right panel). Means and significances calculated by the unpaired Student's *t* test are shown. *P ≤ 0.05; **P ≤ 0.01.

Figure 7. Stromal LTα-LTβR signaling is crucial for maintaining FDC structures and drives *Eμ-Tcl1* leukemia progression. (**A** and **B**) *In vivo* blockage of the LTβR signaling pathway by treatment of *Eμ-Tcl1* mice with 100 μg LTβR-Ig (n=9; right) i.p. in 7 day intervals starting on day -1 up to day 35 or control mouse IgG1 (MOCP21) (n=9; left). Tumor load was assessed at day 0 and 38 in PB (**A**), and at day 38 in (**B**) spleens.

Error bars indicate mean ± SEM. P values in (**A**) were determined by Wilcoxon signed rank test; in (**B**), a Mann-Whitney test was applied. (**C**) Spleen sections (day 38) were stained for $B220^+$ B cells, $CD21^+CD35^+$ FDC networks and CXCL13 expression. A representative section of each group is shown. Scale bar, 50 μm. (**D**) Splenic CCL19, CCL21, CXCL12, and CXCL13 mRNA expression of *Eμ-Tcl1* mice treated with either LTβR-Ig (n=9) or control Ig (n=9) were analyzed by RT-qPCR. Gene expression was calculated relative to Gapdh. Error bars indicate mean ± SEM. P values were determined by a Mann-Whitney test. *P ≤ 0.05; **P ≤ 0.01; ***P ≤ 0.001. (**E**) qRT-PCR of lymphotoxin and TNFα transcripts in sorted human (hu) B cells ($CD19^+$; n=4), hu CLL B cells ($CD19^+CD5^+$; n=3), and in the B-CLL cell line MEC-1 (n=2). Transcript expression was normalized to GAPDH. Error bars indicate mean ± SEM. **(F)** One x 10^7 human MEC-1 cells were i.v. transferred into *NOD/SCID/c-γ-chain*$^{-/-}$ mice. On day 3 up to day 25, mice were treated with 100 μg LTβR-Ig (n=3; right) i.p. in 7 day intervals, or control mouse IgG1 (MOCP21) (n=4; left). Representative spleen sections were stained 28 days after transfer for $CD19^+$ MEC-1 cells (red) and $CD21^+CD35^+$ FDCs (red). Scale bars, 50 μm.

Figure 1

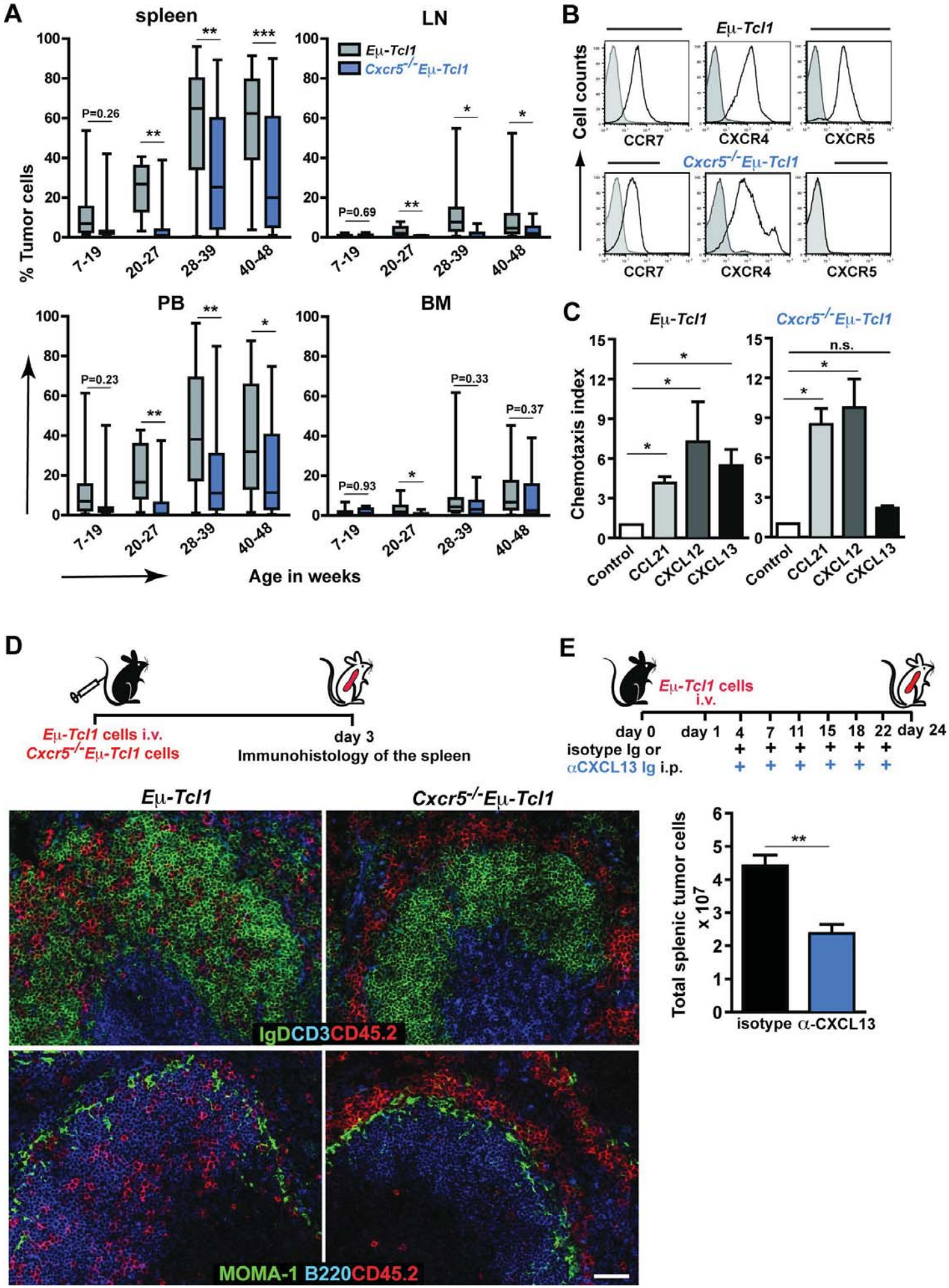
A
spleen
LN
Eμ-Tcl1
Cxcr5-/-Eμ-Tcl1
% Tumor cells
P=0.26
P=0.69
PB
BM
P=0.23
P=0.93
P=0.33
P=0.37
7-19
20-27
28-39
40-48
Age in weeks
B
Eμ-Tcl1
Cxcr5-/-Eμ-Tcl1
Cell counts
CCR7
CXCR4
CXCR5
C
Eμ-Tcl1
Cxcr5-/-Eμ-Tcl1
Chemotaxis index
n.s.
Control
CCL21
CXCL12
CXCL13
D
Eμ-Tcl1 cells i.v.
Cxcr5-/-Eμ-Tcl1 cells
day 3
Immunohistology of the spleen
E
Eμ-Tcl1 cells i.v.
day 0
day 1
4
7
11
15
18
22
day 24
isotype Ig or
αCXCL13 Ig i.p.
Eμ-Tcl1
Cxcr5-/-Eμ-Tcl1
IgDCD3CD45.2
MOMA-1 B220CD45.2
Total splenic tumor cells x 10^7
isotype
α-CXCL13

Figure 2

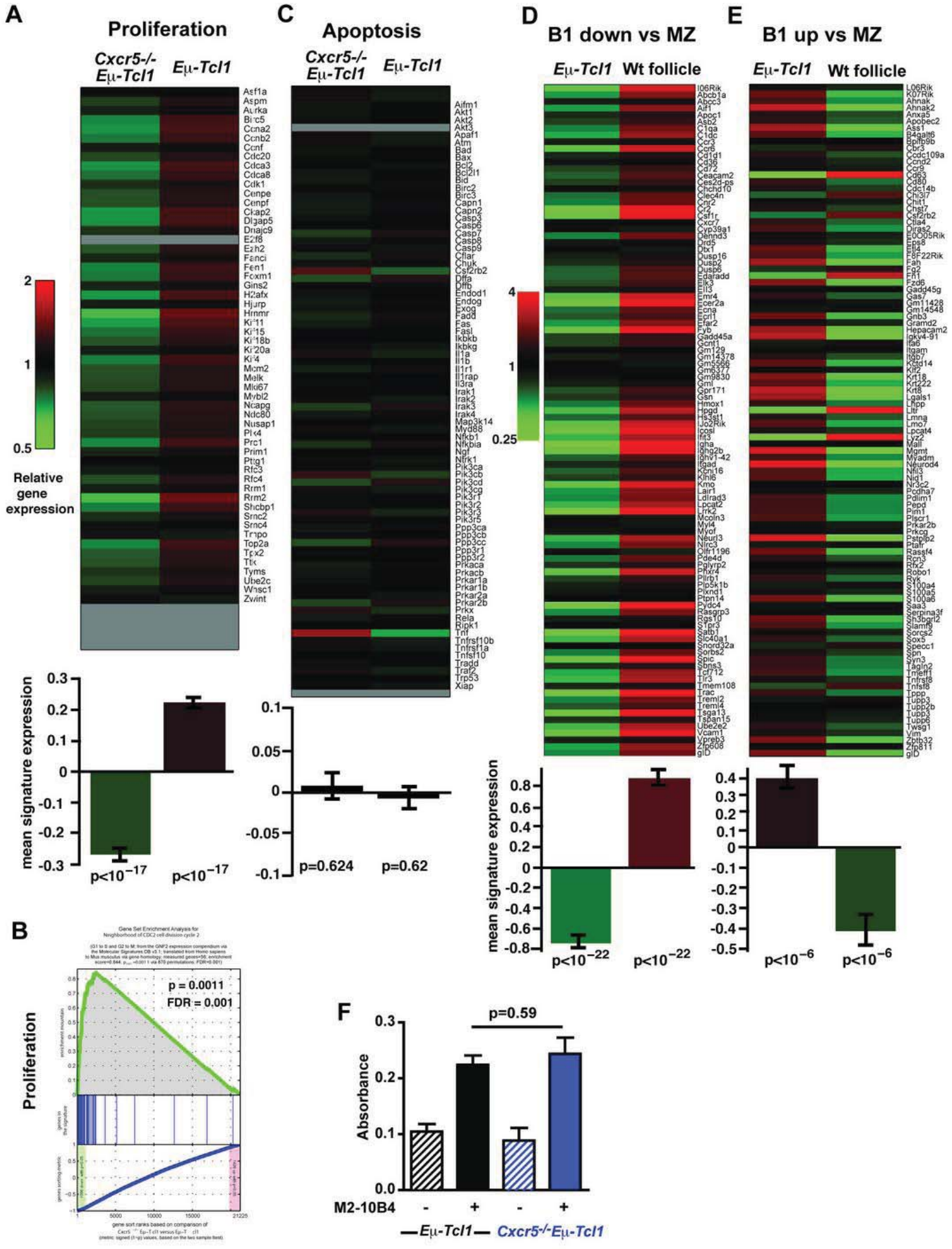
A
Proliferation
Cxcr5-/- Eμ-Tcl1
Eμ-Tcl1
Relative gene expression
mean signature expression
p<10−17
p<10−17
C
Apoptosis
p=0.624
p=0.62
D
B1 down vs MZ
Eμ-Tcl1
Wt follicle
p<10−22
p<10−22
E
B1 up vs MZ
p<10−6
p<10−6
B
Proliferation
p = 0.0011
FDR = 0.001
F
p=0.59
Absorbance
M2-10B4
Eμ-Tcl1
Cxcr5-/-Eμ-Tcl1

Figure 3

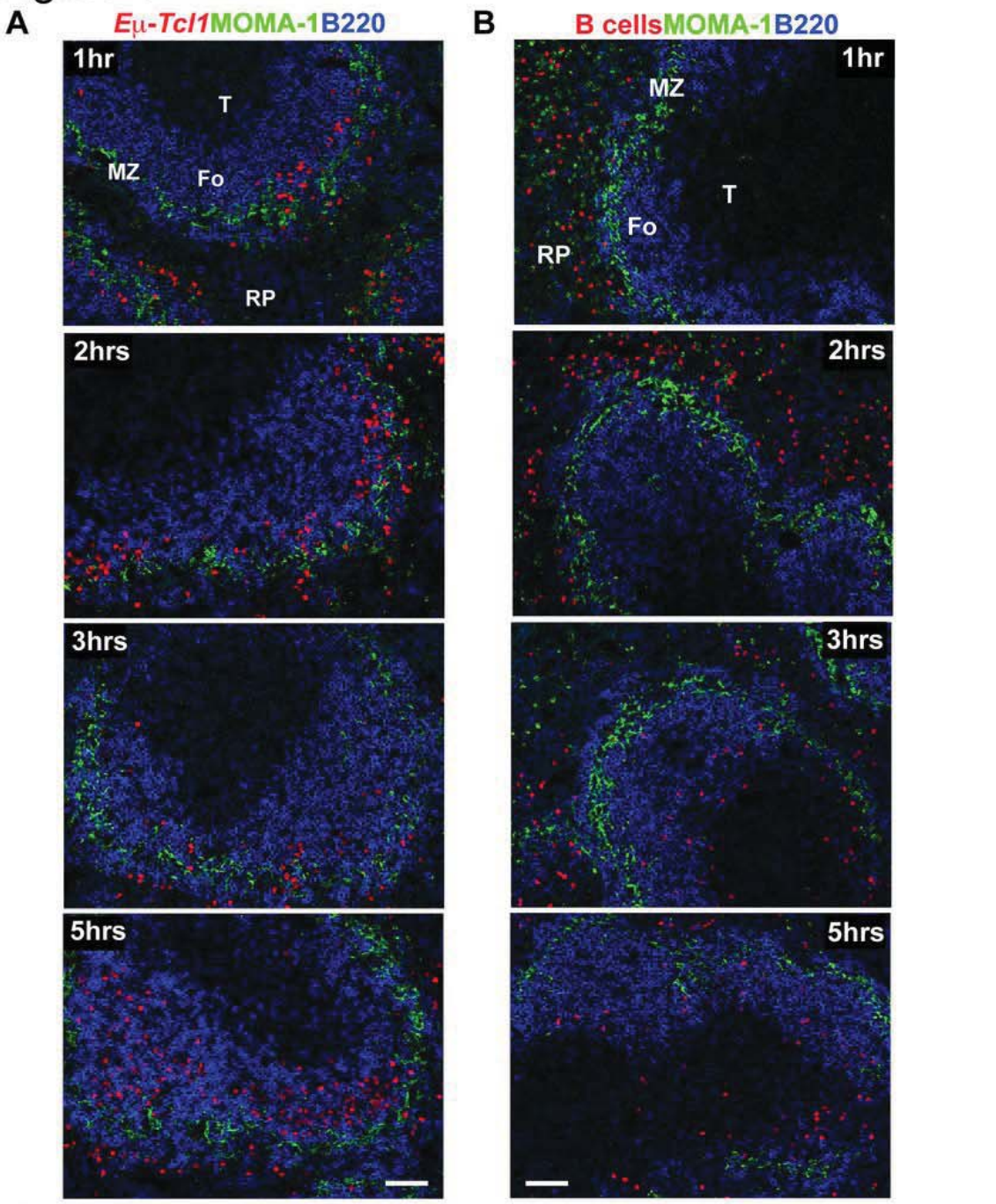
A
Eμ-Tcl1MOMA-1B220
1hr
T
MZ
Fo
RP
2hrs
3hrs
5hrs
B
B cellsMOMA-1B220
1hr
MZ
T
Fo
RP
2hrs
3hrs
5hrs

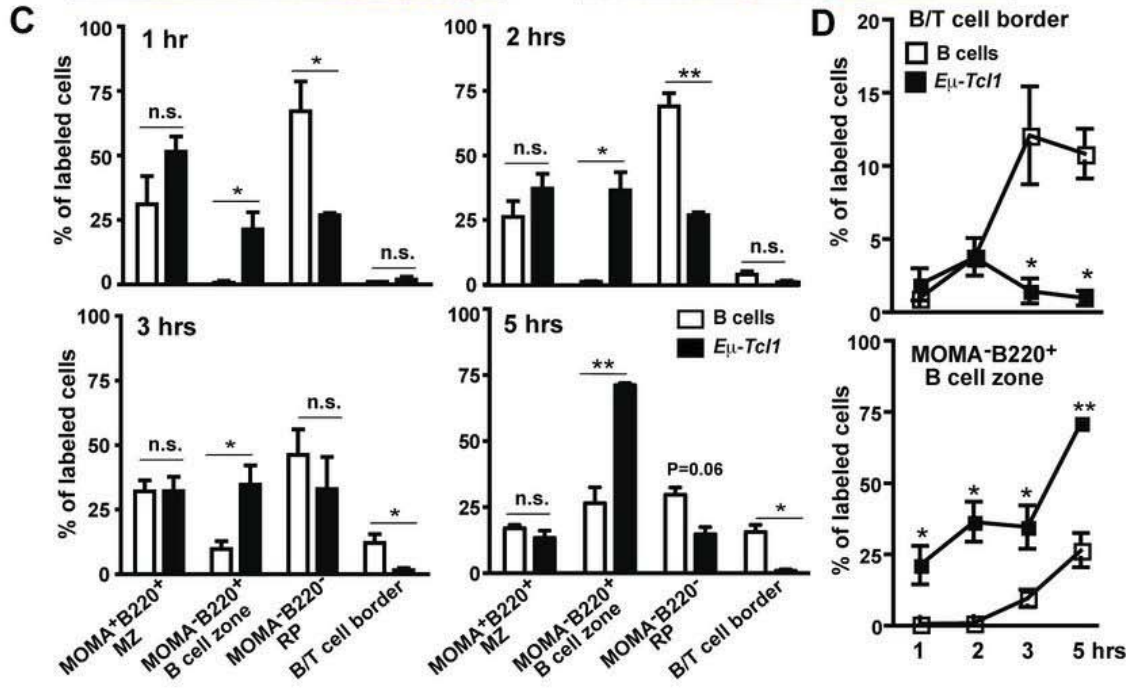
C
1 hr
2 hrs
3 hrs
5 hrs
% of labeled cells
n.s.
*
**
P=0.06
B cells
Eμ-Tcl1
MOMA+B220+ MZ
MOMA-B220+ B cell zone
MOMA-B220- RP
B/T cell border
D
B/T cell border
B cells
Eμ-Tcl1
MOMA-B220+ B cell zone
1
2
3
5 hrs

Figure 4

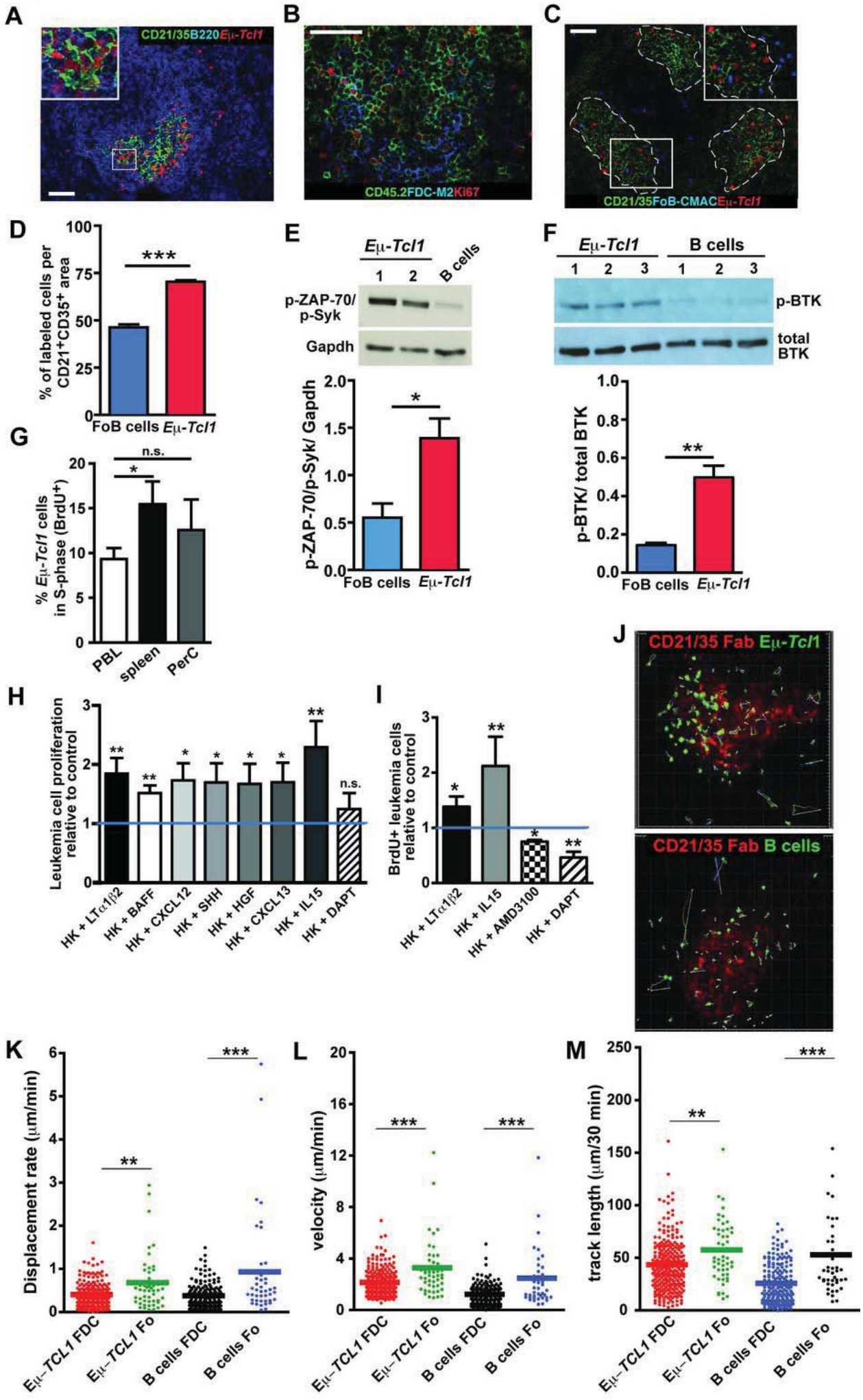
A
CD21/35B220Eμ-Tcl1
B
CD45.2FDC-M2Ki67
C
CD21/35FoB-CMACEμ-Tcl1
D
% of labeled cells per CD21+CD35+ area
***
FoB cells Eμ-Tcl1
E
Eμ-Tcl1
1 2 B cells
p-ZAP-70/ p-Syk
Gapdh
p-ZAP-70/p-Syk/ Gapdh
*
FoB cells Eμ-Tcl1
F
Eμ-Tcl1 B cells
1 2 3 1 2 3
p-BTK
total BTK
p-BTK/ total BTK
**
FoB cells Eμ-Tcl1
G
% Eμ-Tcl1 cells in S-phase (BrdU+)
n.s.
*
PBL spleen PerC
H
Leukemia cell proliferation relative to control
HK + LTα1β2
HK + BAFF
HK + CXCL12
HK + SHH
HK + HGF
HK + CXCL13
HK + IL15
HK + DAPT
I
BrdU+ leukemia cells relative to control
HK + LTα1β2
HK + IL15
HK + AMD3100
HK + DAPT
J
CD21/35 Fab Eμ-Tcl1
CD21/35 Fab B cells
K
Displacement rate (μm/min)
**
***
Eμ–TCL1 FDC
Eμ–TCL1 Fo
B cells FDC
B cells Fo
L
velocity (μm/min)
***
***
Eμ–TCL1 FDC
Eμ–TCL1 Fo
B cells FDC
B cells Fo
M
track length (μm/30 min)
**
***
Eμ–TCL1 FDC
Eμ–TCL1 Fo
B cells FDC
B cells Fo

Figure 5

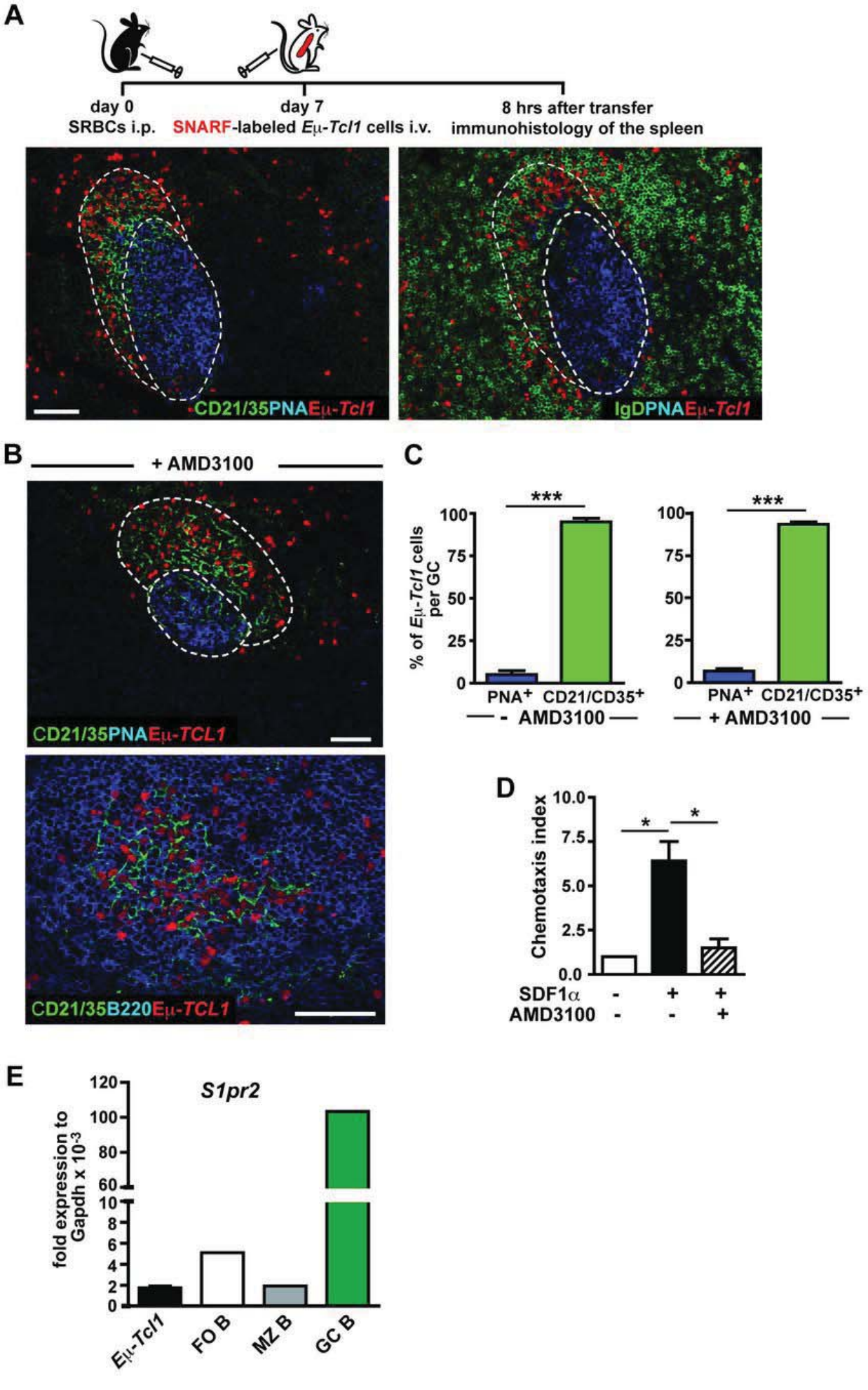
A
day 0
SRBCs i.p.
day 7
SNARF-labeled Eμ-Tcl1 cells i.v.
8 hrs after transfer
immunohistology of the spleen
CD21/35PNAEμ-Tcl1
IgDPNAEμ-Tcl1
B
+ AMD3100
CD21/35PNAEμ-TCL1
CD21/35B220Eμ-TCL1
C
% of Eμ-Tcl1 cells per GC
***
PNA+ CD21/CD35+
- AMD3100
+ AMD3100
D
Chemotaxis index
SDF1α
AMD3100
E
S1pr2
fold expression to Gapdh x 10-3
Eμ-Tcl1
FO B
MZ B
GC B

Figure 6

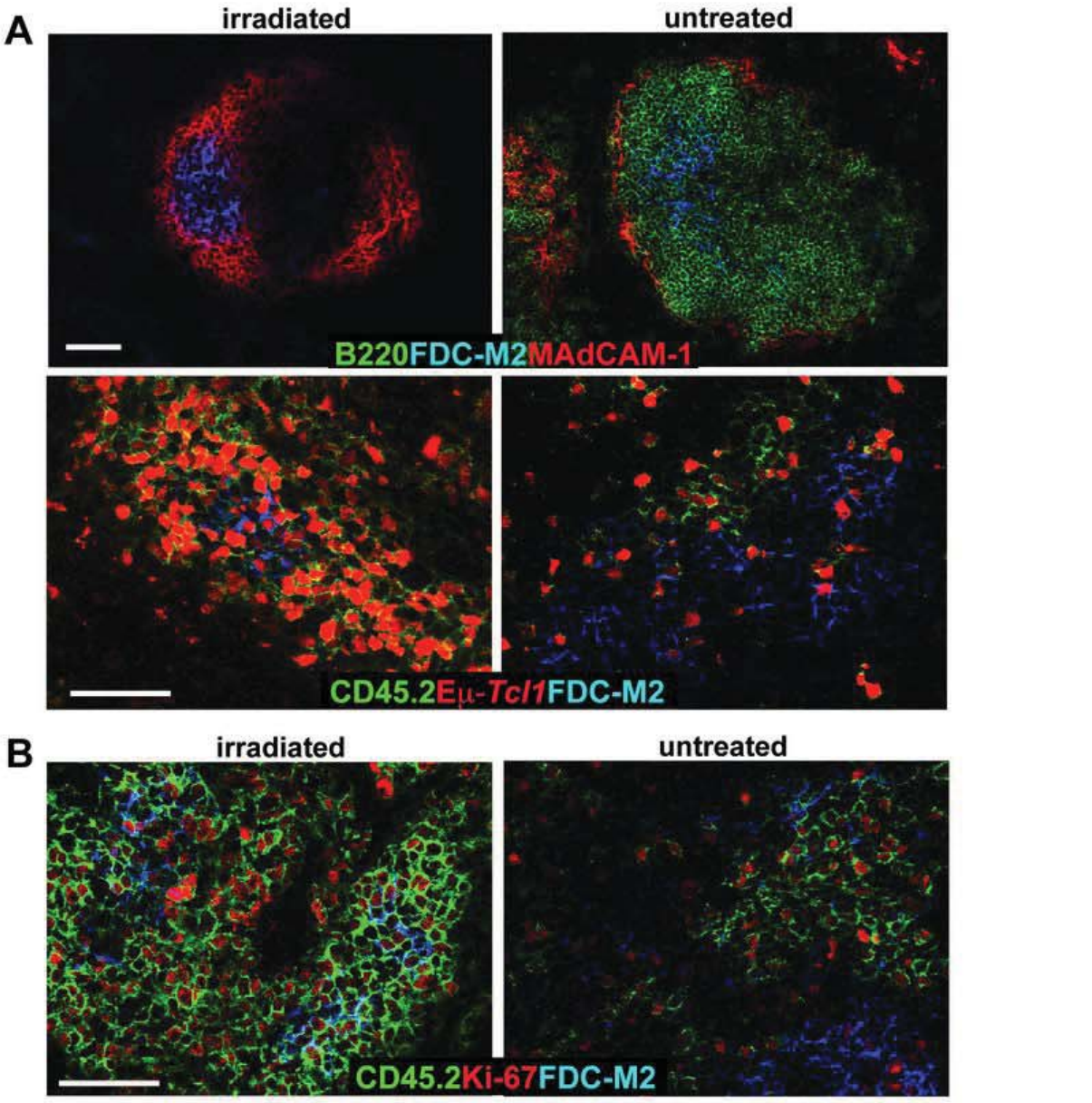
A
irradiated
untreated
B220FDC-M2MAdCAM-1
CD45.2Eμ-Tcl1FDC-M2
B
irradiated
untreated
CD45.2Ki-67FDC-M2
C
untreated
irradiated
Cell counts
Eμ-Tcl1 eFluor670
D
BAFF
APRIL
fold expression to GAPDH
irradiated
Eμ-Tcl1
E
Eμ-Tcl1
Cell counts
BAFFR
F
irradiated
irradiated + α-BAFF
Cell counts
Eμ-Tcl1 eFluor670
% proliferation relative to control
irrad.
irrad. +α-BAFF

Figure 7

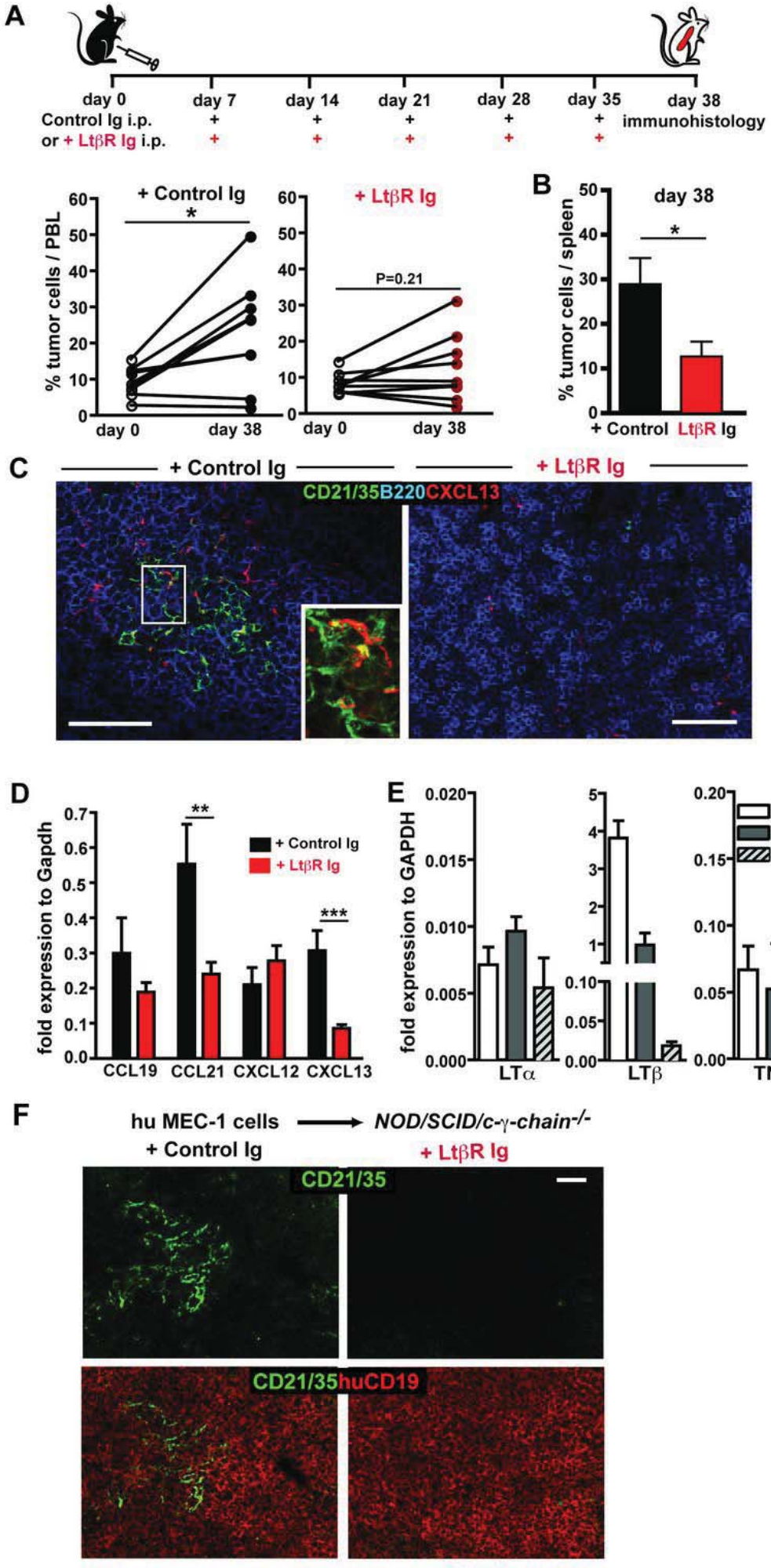
A
day 0
day 7
day 14
day 21
day 28
day 35
day 38
Control Ig i.p.
or + LtβR Ig i.p.
immunohistology
+ Control Ig
+ LtβR Ig
% tumor cells / PBL
P=0.21
B
day 38
% tumor cells / spleen
+ Control
LtβR Ig
C
+ Control Ig
+ LtβR Ig
CD21/35B220CXCL13
D
fold expression to Gapdh
+ Control Ig
+ LtβR Ig
CCL19
CCL21
CXCL12
CXCL13
E
fold expression to GAPDH
hu B cells
hu CLL
hu MEC-1
LTα
LTβ
TNFα
F
hu MEC-1 cells
NOD/SCID/c-γ-chain-/-
+ Control Ig
+ LtβR Ig
CD21/35
CD21/35huCD19

Supplemental Information

Supplemental Methods

Mice

Eμ-Tcl1 transgenic mice on a mixed C3H/C57.BL/6 background were provided by Carlo Croce (1). *Eμ-Tcl1* mice were backcrossed onto a C57BL/6 background for 10 generations. C57BL/6 Ly5.1 (CD45.1) congenic and severe combined immunodeficient common gamma chain mice (*NOD/SCID/c-γ-chain*$^{-/-}$*)* were obtained from Charles River (Sulzfeld, Germany). *Cxcr5*$^{-/-}$ and *Ccr7*$^{-/-}$ mice were generated as described (2, 3) and backcrossed onto a C57BL/6 background for 12 generations. Lymphotoxin (*Lt)* $\alpha^{-/-}$ mice were obtained from Jackson Laboratories (Bar Harbor, ME). EBI2-deficient mice (also referred to as *Gpr183*$^{-/-}$) were generated as described (4); *Ebi2*$^{-/-}$, *Ccr7*$^{-/-}$, *Cxcr5*$^{-/-}$, and *Lt*$\alpha^{-/-}$ mice were crossed with *Eμ-Tcl1* transgenic mice to generate double transgenic mice. C57BL/6-Tg (IghelMD4)4Ccg/J mice carry the transgenic IghelMD4 B cell receptor that recognizes hen egg lysozyme (5); the receptor is further referred to as BCR^{HEL}. About 80-90% of IgM^{+} and IgD^{+} B cells in the spleen are derived from the transgene and exhibit the a allotype; this strain was obtained backcrossed for more than 12 generations (Jackson Laboratories) and then further backcrossed with *Eμ-Tcl1* mice (F10) to obtain double-transgenic *Eμ-Tcl1/*BCR^{HEL} animals. All animal studies were performed according to institutional and Berlin State guidelines.

Antibodies

The following primary antibodies were used for flow cytometry: fluorescein isothiocyanate (FITC) or Pacific Blue (PB)-labeled rat anti-mouse CD19, Biotin labeled rat anti-mouse CCR7; FITC-labeled rat anti-mouse CD62L and CD18, Alexa Fluor (AF) 647-labeled mouse anti-human TCL1; phycoerythrin (PE)-labeled rat anti-mouse LFA-1,

PE-labeled rat anti-mouse CD268 (BAFF-R), biotinylated rat anti-mouse CD29, CD49d and integrin β7, PE-labeled mouse anti-human CD19, FITC-labeled mouse anti-human CD19, PB or AF 647-labeled mouse anti-human CD5 (Biolegend), PE-labeled rat anti-mouse CXCR4 and CXCR5, FITC or allophycocyanin (APC)-labeled rat anti-mouse CD5, and PE-labeled rat anti-mouse CD4, and PE-labeled rat anti-T- and B-cell activation antigen (GL-7) (BD Biosciences). Streptavidin-PE conjugates were used for the detection of biotinylated primary antibodies (Molecular Probes).

For immunohistology the following primary antibodies were used: FITC-labeled anti-mouse MOMA-1, Biotin labeled rat anti-mouse FDC-M2 (Serotec); purified rat anti-mouse Ki67 (Dako); Biotin labeled mouse anti-mouse CD45.2; FITC-labeled rat anti-mouse IgD, FITC-labeled CD21/35 (BD Biosciences); PB- labeled rat anti-mouse CD3, PB-labeled rat anti mouse B220, and purified goat anti-mouse CXCL13 (R&D Systems); purified rat anti-mouse MAdCAM-1, PE-labeled mouse anti-mouse CD157 (BP3), AF 488-labeled mouse anti-mouse CD45.2 (Biolegend). Secondary antibodies included: goat anti-rat IgG AF 568 and AF 488 conjugated, goat anti-mouse Alexa Fluor 488, donkey anti-goat Alexa Fluor 568 (Molecular Probes).

Flow cytometry and cell sorting

Flow cytometry gating strategy to characterize and quantitate leukemia *Eμ-Tcl1* cell frequencies or to isolate tumor cells by cell sorting. Leukemic cells derived from spleen, PB, LN, or BM were characterized as $CD19^{+}CD5^{int}$ cells in contrast to $CD19^{-}CD5^{+}$ T cells (T), $CD19^{+}CD5^{-}$ follicular B cells (B), and $CD19^{+}CD5^{hi}$ B-1 B cells (B-1). The frequency of $CD19^{+}CD5^{int}$ cells was calulated based on all cells within the lymphocyte gate.

For flow cytometry analysis, cells were blocked with CD16/32 antibody in flow cytometry buffer (PBS, 0.5% BSA), followed by staining with the antibodies listed above. Data were acquired on a FACSCantoII flow cytometer (BD Biosciences) and were further analyzed with FlowJo software (TreeStar). Cell sorting was done on a FACSAria (BD Biosciences).

***In vitro* cell proliferation assay**

Five x 10^3 bone marrow stromal cells (M2-10B4; ATCC) per well of a 96 well plate were grown overnight. 1x10^5 splenic-derived *Eμ-Tcl1* or *Cxcr5*$^{-/-}$*Eμ-Tcl1* leukemia cells were seeded per well with or without a stromal cell layer and grown for 48 hours (triplicates). The number of living cells per well was determined using the Cell Titer 96 AQ_{eous} One Solution Cell Proliferation Assay (Promega). Generation of a Formazan product was measured at 450 nm in a 96 well plate reader and proliferation was calculated by subtracting the blank.

For the co-culture of the FDC/HK cell line with individual *Eμ-Tcl1* leukemia cell clones or CLL cells obtained from patient peripheral blood samples, 2x10^3 stroma cells per well were seeded in 96-well plates in RPMI 1640 medium (PAA Laboratories), supplemented with 5% FCS, penicillin-streptomycin, glutamine, and Na-pyruvate (Invitrogen). After adherence, cells were supplemented with 50 ng/ml human LTα1β2, where indicated. Following overnight culture, stroma cells were irradiated with 2000 rad. Next, 1x10^5 leukemia B cells were added in triplicates and mean values were calculated. *Eμ-Tcl1* leukemia cell co-cultures were supplemented with the following murine cytokines, a γ-secretase inhibitor (DAPT) or a CXCR4 antagonist: B-cell activation factor belonging to the TNF family (BAFF), 1 μg/ml (R&D); CXCL13, 500 ng/ml; CXCL12, 100 ng/ml; IL-15, 100 ng/ml; hepatocyte growth factor (HGF), 200 ng/ml; sonic hedgehog (SHH), 200

ng/ml (all from Peprotech); DAPT, 25 μM (Selleckchem); AMD3100 octahydrochloride hydrate, 10 μg/ml (Sigma). After 72 hrs, viable leukemia cells were counted by Trypan Blue exclusion in a Neubauer chamber using light microscopy. Proliferation of leukemia cells grown in the presence of unstimulated FDC/HK cells alone was set arbitrarily at 1. For BrdU incorporation, leukemia cells were supplemented with 10 μM BrdU (Sigma) 24 and 48 hrs after the start of the co-culture.

Peripheral blood samples from treatment naïve CLL patients were purified over a Ficoll gradient. Human CLL cell co-cultures were supplemented with human IL-15, 100 ng/ml (Peprotech); DAPT, 25 μM (Selleckchem) or AMD3100, 10 μg/ml (Sigma). After 24 hrs and 72 hrs the co-cultures were supplemented with 10 μM BrdU. After 96 hrs BrdU incorporation into the DNA was analyzed by flow cytometry with the BrdU Flow Kit (BD Biosciences). CLL cells were gated for $CD19^{+}CD5^{+}BrdU^{+}$ expression.

In vivo cell proliferation

For *in vivo* cell proliferation analysis, splenic-derived *Eμ-Tcl1* leukemia cells were labeled with 1μM Cell Proliferation Dye eFluor670 (eBiosciences) in PBS for 10 min at 37°C. Labeled cells (5 - 10 x 10^6) were adoptively transferred into irradiated C57BL/6 mice together with 50 μg inhibitory polyclonal rabbit anti-BAFF antibody (R&D) or together with the isotype control (Biolegend). 48 hrs after transfer, cells were analyzed by Flow Cytometry.

Alternatively, BrdU incorporation into the DNA of proliferating cells was analyzed by flow cytometry with the BrdU Flow Kit (BD Biosciences). One mg BrdU was injected intraperitoneally (i.p.) in 24 hrs intervals for 3 days.

Immunizations and screening of *Eμ-Tcl1*/BCR^{HEL} double-transgenic mice

BCR^{HEL} expression was determined in mice PB or spleen after repeated immunization with hen egg lysoszme (HEL) by staining B cells with an antibody to IgM^a and IgD^a, an allotypic marker that allows for the identification of BCR^{HEL}-expressing B220^{high} B cells or CD5$^+$ CD19$^+$ leukemia cells. Immunizations with 100-250 μg HEL in Sigma Adjuvant (Sigma) was done in 3-4 weekly intervals by i.p. injections starting at an age of 8-10 weeks. Observation periods were 3-8 months.

Chemotaxis assay. Chemotaxis assays were performed in 5-μm-pore transwell plates (Corning) for 4 hr at 37°C, exactly as described (6). CCL21, CXCL12 and CXCL13 were used at a concentration of 100 nM, 25 nM and 300 nM, respectively (R&D Research Diagnostics).

Human tissue specimen and immunohistochemistry

Formalin-fixed and paraffin-embedded biopsy specimens of 15 cases of CLL were retrieved from the archives of the Institute of Pathology, Charité-Universitätsmedizin Berlin. Four micrometer sections of paraffin-embedded tissue specimens were used for immunohistochemistry.

In brief, dewaxed and rehydrated tissue sections were subjected to antigen retrieval through 2-min submersion in citrate-buffered saline at pH 6.0 in a high-pressure cooker. The primary antibodies rat anti-human CXCR5 (clone 51505; R&D), mouse anti-human CD21 (clone 1F8; Dako), and isotype matched control antibodies were used in a 1:50 dilution and applied for 1 hr. Incubation with a biotinylated secondary antibody for 30 min was followed by adding streptavidin-coupled alkaline phosphatase. Fast Red was used as an alkaline phosphatase substrate (all components were from Dako).

Immunohistology

For frozen sections, tissues were frozen in Tissue Tek OCT compound (Sakura Finetek). Cryosections of 6 μm thickness were cut, air dried, and fixed for 10 min in -20°C acetone. For immunofluorescence, sections were blocked for 30 min with 10% normal rat, goat or donkey serum, respectively; slides were stained for 1.5 hrs at room temperature with biotinylated or fluorescently labeled antibodies. For indirect staining, secondary antibodies were incubated for 1 hr. Biotinylated primary antibodies were detected with streptavidin Alexa Fluor 488 or -568 (Molecular Probes). All slides were mounted in DABCO-Mowiol solution.

Sequential static imaging

Splenic leukemia cells derived from diseased *Eμ-Tcl1* mice or splenic B lymphocytes derived from C57BL/6 mice were sorted and labeled with 2.5 μM SNARF-1 (Molecular Probes) in PBS/ 2%FCS for 15 min at room temperature or with 10 μM CMAC in serum-free medium for 30 min at 37°C, respectively. Labeled cells (1-2 x 10^7) were adoptively transferred into C57BL/6 recipients. Spleens were fixed in a 0.05 M phosphate buffer (pH 7.4) containing 10 mg/ml paraformaldehyde, 2 mg/ml $NaIO_4$ and 0.1 M L-lysin (all Sigma-Aldrich) for 12 hrs and dehydrated in 30 % sucrose in phosphate buffer and frozen in Tissue Tek OCT compound. Staining of cryosections was performed as aforementioned.

Immunofluorescence image acquisition

Fluorescently labeled tissue sections were analyzed on a Zeiss Axio Imager M2m microscope, equipped with an Apo Tome 2.0 (Carl Zeiss). Images were obtained with a 40 x Plan-Apochromat NA 0.9 objective, or a 20 x Plan-Apochromat NA 0.8 objective.

Digital images were processed with Axio Vision 4.8.2 software (Carl Zeiss) and Adobe Photoshop applying the Autocontrast function. Serial z stacks were obtained at 0.3 μm intervals. For quantitative image analysis, ImageJ 1.440 software was used.

Two photon (2P) microscopy

Tumor cells and B lymphocytes were purified applying FACS or magnetic bead separation (Pan B cell isolation Kit, Miltenyi Biotech), respectively and labeled with 2.5 μM SNARF-1. *In vivo* labeling of FDCs was done by Fab-fragments prepared from antibodies against murine CD21/CD35 (clone 7G6) by digestion with immobilized papain. Complete digestion was confirmed by SDS-PAGE. Fab-fragments were labeled with AF568 succinimidyl esters. Five x 10^6 labeled tumor cells or 1 x 10^7 labeled B lymphocytes were injected i.v. in C57BL/6 mice. After 16 hrs, 10 - 20 μg fluorochrome-labeled Fab-fragments were i.v. injected. Four hours after the injection of Fab-fragments, spleens were analysed.

Spleens were cut into 2-3 mm thick slices and transferred into a perfusion chamber (POC-R2 Chamber; H.Saur) with 37°C medium and a low continuous flow (RPMI 1640 without phenol red, 10 mM Hepes). A LaVision TriMScope with an Olympus upright BX 51 microscope stand and an Olympus 20x, NA 0.95 objective were used for imaging. The microscope was equipped with a Coherent Ultra II Ti:Sa Laser. The bandpass filters used for detection of SNARF-1 and FITC were 593/40 and 520/40 nm, respectively. Detection of CFDA and AF568 was done in high sensitivity PMTs after emitted light passed through a 560 nm dicroic mirror and 624/40 bandpass filter. Viability of transferred tumor cells was >90%, as confirmed by AnnexinV- and 7-AAD staining.

For 4D analysis of cell migration, regions covering FDC rich areas and follicular areas (300 x 300 μm) were imaged. Stacks of 3 μm in z- direction were recorded in 16 optical

sections every 60 sec over 30 min at a laser wavelength of 790 nm (for detection of SNARF-1 and FITC) or 806 nm (for detection of CFDA and AF568). Image acquisition was performed with the ImSpector Imaging Software and cell tracking was done using the Imaris 7.4.0 Software (Bitplane).

RNA extraction and RT-PCR

Total RNA of murine leukemia cells, human CLL cells, or the human B-CLL line MEC-1 (DSMZ) was extracted using the RNeasy Mini Kit (Qiagen), and integrity was confirmed with an Agilent Bioanalyzer system. cDNA was synthesized with oligo(dT) primers plus random hexamers using the SuperScript III First-Strand Synthesis System for RT-PCR kit (Invitrogen) or the RT^{2}First Strand Kit (Qiagen). Real-time RT-PCR (RT-qPCR) was performed using the IQ5 Real-Time PCR Detection System (Bio-Rad). PCR reactions contained 100 ng cDNA in a total volume of 25 µl. SYBR Green 1 reagent (Sigma) was used for detection of PCR products. PCR conditions included: 10 min, 95°C activation of Perpetual Taq polymerase (Roboklon), denaturation 10 s, 95°C; annealing 30 s, (temperature according to Supplemental Table 1); elongation 30 s, 72°C; denaturation 1 min, 95°C; melt curve 10 s/0.5°C, range: 55-95°C; 40 cycles.

Sequence specific primers were designed according to the Primer3 Input software 0.4.0 (http://frodo.wi.mit.edu/). For data analysis, gene transcript expression was calculated relative to Gapdh.

For analysis of chemokine expression in whole spleen, total RNA was prepared using the Trizol reagent (Invitrogen) according to the supplied protocol. Isolation of mRNA was performed with the RNeasy purification Kit (Qiagen). The mRNA expression was calculated relative to Gapdh. Expression of Runx2 and p21 was assessed using the Mouse Sonic Hedgehog Signaling Pathway PCR Array or a p21 Primer Assay,

respectively (SA Bioscience/Qiagen). Messenger RNA expression was calculated relative to house keeping genes suggested by the manufacturer.

Gene expression profiling

Gene expression profiling in splenic-derived *Eμ-Tcl1* and *Cxcr5*$^{-/-}$*Eμ-Tcl1* leukemia cells was performed after sorting of tumor cells (CD5^{+}CD19^{+}) from diseased animals of each genotype with an average tumor load in the spleen of 21.5% (range 15-40% of all lymphocytes). Tumor cell purity after sorting was > 95% and RNA was extracted as described above. For each sample, 30 ng of RNA were used for cDNA synthesis and amplification employing the Ovation® Pico WTA System V2 (NuGEN). Fragmentation and labeling of cDNA was performed using the Encore™ Biotin Module (NuGEN). Labeled transcripts were hybridized to Affymetrix Mouse Gene 1.1 ST microarrays and processed automatically using the Affymetrix GeneTitan system. Raw signal intensities were quantile-normalized and a group effect between the two measurement charges was neutralized (mean expressions of *Eμ-Tcl1* samples and *Cxcr5*$^{-/-}$*Eμ-Tcl1* samples were equalized across groups, keeping the relative $\log_2$ intensities inside each measurement group). Probes were aggregated on gene level using median polish based on probe sets defined in version 14.1.0 of the Entrez Gene custom CDF from (7). Differential genes of *Cxcr5*$^{-/-}$*Eμ-Tcl1* versus *Eμ-Tcl1* leukemia cells were identified using a two-sample t-test, assuming equal expression variance in each genotype.

Gene Set Enrichment Analysis (GSEA)

Enrichment analysis was employed to objectively identify different regulation of pathway-associated sets of genes. GSEA was performed as described previously (8) against an integrated database containing the Molecular Signature Database v3.1 (9), the

GeneSigDB (10) and the Staudt Lab library (11). Signatures of human genes were translated via gene homology data. Only those gene signatures that obtained a significant ($p < 0.005$, FDR < 5%) enrichment score as well as those that contained at least 20% significantly differentially expressed genes ($p < 0.05$, 2-sample t-tests) were considered to represent differentially regulated pathways between the two genotypes investigated. Signatures with less than 10 genes were filtered out. Heatmaps of selected signatures show for each genotype and each gene the genotype-averaged $\log_2$(ratio) with respect to the mean expression across all samples. Bars beneath each column represent the average $\log_2$(ratio) of the signature. Error bars depict standard errors of the mean. P values are calculated for the null hypothesis that the signature is not regulated for the respective sample (paired t-test against zero $\log_2$(ratio)).

We also performed gene expression profiling of B-1 B cells and marginal zone (MZ) B cells and defined two gene expression signatures comprised of the top 100 downregulated and the top 100 upregulated genes in B-1 cells compared to MZ B cells. We then analyzed gene expression of these signatures in tumor cells derived from transgenic *Eμ-Tcl1* mice versus cells derived from healthy Wt mice. These cells were obtained by laser-microdissection of splenic folllicular B cell areas using the PixCell IIe LCM System (Arcturus).

Antibodies for immunoblot analysis

The following primary antibodies were used for immunoblot analysis: anti-phospho-pZAP-70(Tyr319/pSyk(Tyr352), anti-phospho-p44/42 MAPK (Erk1/2)(Thr202/Tyr204), anti-p44/42 MAPK(Erk1/2), anti-phospho-Akt, anti-Akt (Pan) (C67E7), anti-phospho-p38 MAPK(Thr180/Tyr182), anti-p38 MAPK (D13E1) XP®, anti-phospho-pBTK

(Tyr233), anti-BTK (Cell Signaling); anti-Calnexin (Enzo Life Science) or anti-GAPDH (Abcam) were used as loading controls.

Immunoblot analysis

$1x10^4$ follicular dendritic cell line FDC/HK (12) per well of a 24 well plate were grown overnight. $1x10^6$ splenic *Eμ-Tcl1* or *Cxcr5*$^{-/-}$*Eμ-Tcl1* leukemia cells derived from highly diseased mice were seeded per well and grown for 72 hours. Alternatively, splenic $CD5^+CD19^+$ leukemia cells were FACS sorted from spleens of *Eμ-Tcl1* transgenic animals with a tumor load of 8-20% in the blood and splenic $CD19^+$ B cells were sorted from naive Wt mice. The lymphoma and B cell lysates were generated in lysis buffer (20 mM Hepes, pH 7.9, 350 mM NaCl, 1% Nonidet P-40, 1 mM $MgCl_2$, 0.5 mM EDTA, 0.1 mM EGTA, 1 mM phenylmethylsulfonylfluorid, 5 μg/ml aprotinin, 10 mM NaF, 1 mM Na_3VO_4, 2 mM β-glycerolphosphate). Proteins were analyzed by immunoblot and visualized by chemiluminescence (ECL kit, Thermo Scientific). Densitometric quantification of gel bands was performed using the ImageJ 1.440 software.

Densitometric quantification of gel bands was performed using the ImageJ 1.440 software.

Supplemental References

1. Bichi R, Shinton SA, Martin ES, Koval A, Calin GA, Cesari R, et al. Human chronic lymphocytic leukemia modeled in mouse by targeted TCL1 expression. Proc Natl Acad Sci U S A. 2002 May 14;99(10):6955-60. PubMed PMID: 12011454. Epub 2002/05/16. eng.
2. Förster R, Mattis AE, Kremmer E, Wolf E, Brem G, Lipp M. A putative chemokine receptor, BLR1, directs B cell migration to defined lymphoid organs and specific anatomic compartments of the spleen. Cell. 1996 Dec 13;87(6):1037-47. PubMed PMID: 8978608. Epub 1996/12/13. eng.
3. Förster R, Schubel A, Breitfeld D, Kremmer E, Renner-Muller I, Wolf E, et al. CCR7 coordinates the primary immune response by establishing functional microenvironments in secondary lymphoid organs. Cell. 1999 Oct 1;99(1):23-33. PubMed PMID: 10520991. Epub 1999/10/16. eng.
4. Gatto D, Paus D, Basten A, Mackay CR, Brink R. Guidance of B cells by the orphan G protein-coupled receptor EBI2 shapes humoral immune responses. Immunity. 2009 Aug 21;31(2):259-69. PubMed PMID: 19615922. Epub 2009/07/21. eng.
5. Goodnow CC, Crosbie J, Adelstein S, Lavoie TB, Smith-Gill SJ, Brink RA, et al. Altered immunoglobulin expression and functional silencing of self-reactive B lymphocytes in transgenic mice. Nature. 1988 Aug 25;334(6184):676-82. PubMed PMID: 3261841. Epub 1988/08/25. eng.
6. Höpken UE, Foss HD, Meyer D, Hinz M, Leder K, Stein H, et al. Up-regulation of the chemokine receptor CCR7 in classical but not in lymphocyte-predominant Hodgkin disease correlates with distinct dissemination of neoplastic cells in lymphoid organs. Blood. 2002 Feb 15;99(4):1109-16. PubMed PMID: 11830455. Epub 2002/02/07. eng.
7. Dai M, Wang P, Boyd AD, Kostov G, Athey B, Jones EG, et al. Evolving gene/transcript definitions significantly alter the interpretation of GeneChip data. Nucleic Acids Res. 2005;33(20):e175. PubMed PMID: 16284200. Epub 2005/11/15. eng.
8. Subramanian A, Tamayo P, Mootha VK, Mukherjee S, Ebert BL, Gillette MA, et al. Gene set enrichment analysis: a knowledge-based approach for interpreting genome-wide expression profiles. Proc Natl Acad Sci U S A. 2005 Oct 25;102(43):15545-50. PubMed PMID: 16199517. Epub 2005/10/04. eng.
9. Liberzon A, Subramanian A, Pinchback R, Thorvaldsdottir H, Tamayo P, Mesirov JP. Molecular signatures database (MSigDB) 3.0. Bioinformatics. 2011 Jun 15;27(12):1739-40. PubMed PMID: 21546393. Epub 2011/05/07. eng.
10. Culhane AC, Schroder MS, Sultana R, Picard SC, Martinelli EN, Kelly C, et al. GeneSigDB: a manually curated database and resource for analysis of gene expression signatures. Nucleic Acids Res. 2011 Jan;40(Database issue):D1060-6. PubMed PMID: 22110038. Epub 2011/11/24. eng.
11. Shaffer AL, Wright G, Yang L, Powell J, Ngo V, Lamy L, et al. A library of gene expression signatures to illuminate normal and pathological lymphoid biology. Immunol Rev. 2006 Apr;210:67-85. PubMed PMID: 16623765. Epub 2006/04/21. eng.
12. Park CS, Yoon SO, Armitage RJ, Choi YS. Follicular dendritic cells produce IL-15 that enhances germinal center B cell proliferation in membrane-bound form. J Immunol. 2004 Dec 1;173(11):6676-83. PubMed PMID: 15557159.

Table S1. Lack of induction of BCR^{HEL}-expressing leukemia B cells in *Eμ-Tcl1*/BCR^{HEL} transgenic mice after repeated immunization with HEL

Mouse No.	Immunization HEL i.p.	$CD5^+CD19^+$ BCR^{HEL+} tumor cells	$CD5^+CD19^+$ BCR^{HEL-} tumor cells (%)	$CD5^-CD19^+$ BCR^{HEL+} B cells
1	6x	-	-	+
2	6x	-	-	+
3	8x	-	-	+
4	9x	-	82	+
5	10x	-	-	+
6	12x	-	33.8	+
7	12x	-	0.8	+
8	12x	-	79.9	+

*BCR^{HEL}-expression was determined in mice after repeated immunization with HEL (as indicated) by staining the cells with an antibody to IgM^a and IgD^a, an allotypic marker that allows for identification of BCR^{HEL}-expressing $B220^{hi}$ B cells or $CD5^+CD19^+$ leukemia cells. Observation period 3-8 months.

Table S2. *Eμ-Tcl1*/BCR^{HEL} transgenic mice exhibit BCR^{HEL}-expressing B220^{hi} B cells but do not develop BCR^{HEL}-expressing leukemia B cells

Mouse No.	Age (weeks)	CD5$^+$CD19$^+$ BCR^{HEL+} tumor cells*	CD5$^+$CD19$^+$ BCR^{HEL-} tumor cells (%)	CD5$^-$CD19$^+$ BCR^{HEL+} B cells*
1	20-27	-	-	+
2	20-27	-	21.0	+
3	20-27	-	-	+
4	20-27	-	-	+
5	20-27	-	9.5	+
6	20-27	-	-	+
7	20-27	-	-	+
8	20-27	-	-	+
9	20-27	-	-	+
10	28-39	-	6.2	+
11	28-39	-	5.3	+
12	28-39	-	-	+
13	28-39	-	21.5	+
14	28-39	-	78.4	+
15	28-39	-	-	+
16	28-39	-	41.3	+
15	28-39	-	-	+
16	28-39	-	62.4	+
17	28-39	-	-	+
18	28-39	-	26.0	+
19	28-39	-	65.0	+
20	28-39	-	-	+
21	28-39	-	-	+
22	28-39	-	-	+
23	28-39	-	-	+
24	28-39	-	-	+
25	28-39	-	2.0	+
26	40-48	-	-	+
27	40-48	-	70.9	+
28	40-48	-	6.32	+
29	40-48	-	93.3	+
30	40-48	-	5.2	+
31	40-48	-	14.3	+

*BCR^{HEL}-expression was determined by staining the cells with an antibody to IgM^a and IgD^a, an allotypic marker that allows for identification of BCR^{HEL}-expressing B220^{hi} B cells or CD5$^+$CD19$^+$ leukemia cells.

Table S3. Oligonucleotides for qRT-PCR

Gene	Sequence	RT^2 Annealing (°C)	$MgCl_2$ (mM)	Primer (μM)
APRIL F2	5′ GTAACCCGCTCTTCCCTTCT 3′	60	2,5	0,25
APRIL R2	5′ GGATCAGTAGTGCGACAGCA 3′			
BAFF F1	5′ TTGTCCAGCAGTTTCACAGC 3′	60-65	2,5	0,25
BAFF R1	5′ CCGGTGTCAGGAGTTTGACT 3′			
BAFFR F1	5′ GGACTGATACTGGCGCTGAC 3′	61	2,5	0,25
BAFFR R1	5′ CACTGCTGCTATTGCTCTGG 3′			
BCMA F1	5′ AACCCTCCTGCAACCTGTC 3′	58-61	2,5	0,25
BCMA R1	5′ CAGCCCTGATCCTAGTCAGC 3′			
CCL19 forw	5′ AGA CTG CTG CCT GTC TGT GA 3′	66,4	2,5	0,25
CCL19 rev	5′ TGC TGT TGC CTT TGT TCT TG 3′			
CCL20 forw	5′ CGACTGTTGCCTCTCGTACA 3′	64,8	3,0	0,5
CCL20 rev	5′ AGGAGGTTCACAGCCCTTTT 3′			
CCL21 forw	5′ GGGCTGCAAGAGAACTGAAC 3′	59	3,0	0,2
CCL21 rev	5′ CCGTGCAGATGTAATGGTTG 3′			
CXCL12 forw	5′ CTTCCACCAGAGCAGAGTCC 3′	66,5	2,0	0,5
CXCL12 rev	5′ GTTTGGAGGCAAGCAGAGAG 3′			
CXCL13 forw	5′ TGACAACCCACTTCAGATGC 3′	65,2	4,0	0,5
CXCL13 rev	5′ GGAAGCCTGCGTTTTACAAAG 3′			
CXCL10 forw	5′ CCCACGTGTTGAGATCATTG 3′	63,3	3,0	0,5
CXCL10 rev	5′ CACTGGGTAAAGGGGAGTGA 3′			
GAPDH forw	5′ AACTTTGGCATTGTGGAAGG 3′	65,2	2,5	0,25
GAPDH rev	5′ ACACATTGGGGGTAGGAACA 3′			
LTα forw	5′ CCC ATC CAC TCC CTC AGA AG 3′	57,3	2,5	0,5
LTα rev	5′ CGCACTGAGGAGAGGCACAT 3′			
LTβ forw	5′ TAT CAC TGT CCT GGC TGT GC 3′	66,4	2,5	0,25
LTβ rev	5′ TGG ATC TCT GAG GAT GCA GA 3′			
TACI F1	5′ CCATCTTCTGCTGTTTCTTGG 3′	61,4	2,5	0,25
TACI R1	5′ CTCCTGAGTGGGAGAACTGC 3′			
TNFα forw	5′ TCTCATCAGTTCTATGGCCC 3	63,5	2,5	0,5
TNFα rev	5′ GGGAGTAGACAAGGTACAAC 3′			

Runx2: Mouse Sonic Hedgehog Signaling Pathway PCR Array (RT^2 Profiler PCR Array System, Qiagen)

p21 (Cdkn1a), S1pr1: Mouse Cdkn1a, mouse S1pr2/ Mouse Gapdh (RT^2 qPCR Primer Assay, Qiagen)

Human LTα, LT, TNFα, and **GAPDH**: RT^2 qPCR Primer Assay, Qiagen

Supplemental Figure Legends

Figure S1. Eμ-*Tcl1* leukemia B cells show a clonal phenotype. (**A**) Flow cytometry gating strategy to characterize and quantitate leukemia *Eμ-Tcl1* cell frequencies. Leukemic cells derived from spleen, PB, LN, and BM were characterized as $CD19^{+}CD5^{int}$ cells in contrast to $CD19^{-}CD5^{+}$ T cells (T), $CD19^{+}CD5^{-}$ follicular B cells (B), and $CD19^{+}CD5^{hi}$ B-1 B cells (B-1). The frequency of $CD19^{+}CD5^{int}$ cells was calulated based on all cells within the lymphocyte gate. Exemplary, splenic cells derived from a diseased *Eμ-Tcl1* transgenic mice are depicted here. Surface expression of IgM and B220 (**B**) or of CD11b and CD86 (**C**) on $CD19^{+}CD5^{int}$ gated tumor cells derived from spleens of leukemic *Eμ-Tcl1* transgenic mice was assessed by flow cytometry. Representative dot plots of two leukemic *Eμ-Tcl1* transgenic mice are shown (n=5 mice analysed per marker (in red); isotype control (in blue). (**D**) Chemokine receptor CCR7, CXCR4, and CXCR5 expression on splenic, LN, PB, and BM derived $CD19^{+}B220^{low}CD5^{+}$ gated *Eμ-Tcl1* tumor cells (n=3-5 mice per marker; isotype control; shaded curve). One representative histogram is shown for each organ and each receptor.

Figure S2. Human CLL tissues and murine Eμ-*Tcl1* leukemia B cells share strong expression of CXCR5. (**A**) Surface expression of adhesion molecules on $CD19^{+}CD5^{int}$ gated tumor cells derived from spleens of leukemic *Eμ-Tcl1* and *Cxcr5*$^{-/-}$*Eμ-Tcl1* transgenic mice was assessed by flow cytometry (n=4-7 mice per marker; isotype control; shaded curve). (**B**) Quantitative RT-PCR of chemokine and lymphotoxin transcripts in sorted tumor cells ($CD19^{+}CD5^{int}$) of *Eμ-Tcl1* (n=3-4) and *Cxcr5*$^{-/-}$*Eμ-Tcl1* (n=3) transgenic mice. Transcript expression was normalized to GAPDH. Error bars indicate mean ± SEM of two independent experiments. (**C**) Detection of CXCR5 in

human CLL specimens *in situ*. Immunohistochemical detection of human CXCR5 on paraffin-embedded sections of a tonsil and LN biopsies of representative CLL cases (n=15). In the tonsil (left), the follicular mantle cell (FoM) area is brightly stained, whereas in the germinal center (GC) only a few CXCR5-positive cells are detectable. In the two representative CLL cases depicted here (right), most of the tumor cells exhibit a robust staining pattern. In CLL case #1, a proliferation center (PC) shows a weak staining for CXCR5, with medium-sized blast cells predominating over small lymphocytes. Magnification, 400x. (**D**) Surface expression of the chemokine receptor CXCR5 on $CD19^{+}CD5^{int}$ gated human peripheral blood CLL cells was assessed by flow cytometry (n=3 CLL cases (#1-3) ; isotype control; shaded curve).

Figure S3. Differential gene expression signatures of *Eμ-Tcl1* versus CXCR5-deficient *Eμ-Tcl1* leukemias. (**A**) Gene expression profiling of fluorescence-activated cell sorted (FACS) *Eμ-Tcl1* (n=6) or *Cxcr5*$^{-/-}$*Eμ-Tcl1* (n=5) leukemia cells ($CD19^{+}CD5^{+}$). Tumor cells were sorted from mice of each group with a splenic tumor load between 10-45% of all lymphocytes, and purity after sorting was > 95%. Enrichment plots of seven proliferation-related signatures are shown which were identified by gene set enrichment analysis to be significantly downregulated and to have an enrichment score of at least 0.5. Blue lines mark genes in the signature; the p value of the enrichment scores, determined by permutation tests, and the false discovery rates are indicated. A table with GSEA top hits is avilable upon request. (**B**) Congenic B6 ($CD45.1^{+}$) mice were adoptively transferred (i.v.) with *Eμ-Tcl1* or CXCR5-deficient *Eμ-Tcl1* leukemia cells ($CD45.2^{+}$). At day 3 after transfer, splenic tumor cells ($CD19^{+}CD5^{+}CD45.2^{+}$) and endogenous B lymphocytes ($CD19^{+}CD5^{-}CD45.2^{-}$) were retrieved by FACS, and RNA derived from these cells was analysed on a Mouse Sonic

Hedgehog Signaling Pathway specific RT-PCR array. Differential gene expression for Wnt6, Wnt10a, and Wnt10b and Runx2 in *Eμ-Tcl1* (n=3) or CXCR5-deficient *Eμ-Tcl1* leukemia cell clones (n=3) compared to gene expression in normal B cells (n=3) is depicted. Gene expression of the cell cycle inhibitor p21 (**C**) was determined by quantitative RT-PCR. Transcript expression was normalized to house keeping genes HKG or GAPDH, respectively. (**D**) Immunoblot analysis of leukemia cell activation and proliferation pathways. $1x10^6$ splenic-derived *Eμ-Tcl1* (n=6 independent clones) or *Cxcr5*$^{-/-}$*Eμ-Tcl1* (n=3 independent clones) leukemia cells were seeded on top of FDC/HK stroma cells. After 72 hrs, leukemia cells were retrieved and lysates were analysed in SDS-PAGE and immunoblot. Membranes were incubated with the antibodies indicated, anti-calnexin served as a loading control. Quantification of the ratios phosphorylated and total kinases is depicted on the right. Error bars indicate mean ± SEM. P values were determined by unpaired Student's *t* test. *P ≤ 0.05; **P ≤ 0.01; n.s., non-significant.

Figure S4. Migratory routes and temporal migration pattern of *Ccr7*$^{-/-}$*Eμ-Tcl1* and *Ebi2*$^{-/-}$*Eμ-Tcl1* leukemia B cells to and within lymphoid follicles.

(A) Splenic *Ccr7*$^{-/-}$*Eμ-Tcl1* leukemia cells ($CD5^+CD19^+$) were purified by FACS and $2x10^7$ SNARF-1 labeled leukemia cells were transferred i.v. into recipient mice. Five and 8 hrs after tumor cell transfer spleens were harvested and localization of tumor cells was analyzed by immunofluorescence stainings (n=2 mice per time point). Spleen sections were stained for MOMA-1^+ metallophilic macrophages (green) and $B220^+$ B cells (blue) to distinguish the MZ (MOMA-1^+B220^+; MZ), the B cell follicle (MOMA-1^-B220^+; Fo), the red pulp (MOMA-1^-B220^-; RP) and T cell zone (MOMA-1^-B220^-; T) at 5 and 8 hrs after transfer (upper panels). Additional stainings for the $CD21^+CD35^+$ FDC network (green) and $B220^+$ B cells (blue) reveal co-localization of the tumor cells with follicular

FDCs 8 hrs after transfer (lower panels). At higher resolution, *Ccr7*$^{-/-}$*Eμ-Tcl1* lymphoma cells were found to intermingle tightly with the CD21^{+}CD35^{+} FDC network. One representative section is shown for each time point and staining. Scale bars, 50 μm.

(**B**) Adoptive transfer of 2 x 10^7 splenic leukemia cells of *Ebi2*$^{-/-}$*Eμ-Tcl1* mice (CD45.2^{+}) into congenic CD45.1^{+} B6 recipients (n=4). Three days after i.v. transfer, spleen sections were stained for CD45.2^{+} tumor cells (red), CD3^{+} T cells (blue), and IgD^{+} B cells (green). (**C**) Splenic follicular B cells (B220^{+}CD21^{int}CD23^{hi}) and *Ebi2*$^{-/-}$*Eμ-Tcl1* lymphoma cells were sorted and labeled with cell tracker dyes CMAC (FoB, blue) and SNARF-1 (leukemia cells, red), respectively. 1x10^7 cells of both groups were co-transferred into recipient mice (n=3). Localization of the differentially labeled cells was analyzed 12 hrs after transfer by co-staining the CD21^{+} CD35^{+} FDC network (green). The FDC rich zones of the B cell follicle are marked by the dashed white line. Scale bar, 100 μm. (**D**) Tumor load in peripheral blood (PB) of 7-19 (n=19), 20-27 (n=17), 28-39 (n=52), and 40-48 (n=52) week-old *Eμ-Tcl1* and 7-19 (n=17), 20-27 (n=18), 28-39 (n=16), and 40-48 (n=4) week-old *Ebi2*$^{-/-}$*Eμ-Tcl1* mice was quantitated by flow cytometry. Tumor cells were defined as CD19^{+}B220^{low}CD5^{+}. Error bars indicate mean ± SEM. Applying the unpaired Student's *t* test, no statistical differences within the age groups were observed.

Figure S5. Lymph node biopsies of CLL patients exhibit FDC networks. Immunohistochemical detection of human FDC networks on paraffin-embedded sections of LN biopsies of representative CLL cases (n=15). Two representative CLL cases are depicted. Magnification, 400 x.

Figure S6. PTX treatment induces *Eμ-Tcl1* cell apoptosis.

(A) On the left, forward scatter (FSC) and side scatter (SSC) profiles of *Eμ-Tcl* lymphoma cells co-cultured with FDC-HK stroma cells for 72 hrs (see Figure legend 4E) with or without PTX is shown. On the right, tumor cell viability was assessed by Annexin-V and 7-AAD staining. Representative dot plots for one clone from 3 independent experiments are shown. (B) One $x10^5$ human CLL leukemia cells were seeded in triplicates on top of unstimulated (control group) or LTα1β2 prestimulated FDC-HK stroma cells alone, or together with Il-15, and the Notch-inhibitor DAPT, as indicated. After 24 and 72 hrs of co-culture, cells were supplemented with 10 μM BrdU and after 96 hrs BrdU incorporation was analyzed by flow cytometry ($CD19^+CD5^+BrdU^+$). Results are shown as x-fold cell survival relative to control (human CLL cells w/o FDC-HK), set arbitrarily to 1 (indicated by a horizontal line; n=3 CLL cases analyzed in independent experiments). Error bars indicate mean ± SEM. P values were determined by the unpaired Student's t test. *P ≤ 0.05; **P ≤ 0.01; n.s., non significant.

Figure S7. *In vivo* staining of the $CD21^+CD35^+$ FDC network.

The $CD21^+CD35^+$ FDC network was visualized by staining with AF568-labeled anti-$CD21^+CD35^+$ Fab fragments (red). Antibodies were applied i.v. 12 hrs before intravital imaging. Sections of frozen spleens were stained additionally with anti-$CD21^+CD35^+$ (green), and follicular $B220^+$ B cells were stained in blue. Scale bar, 50 μm.

Figure S8. *Eμ-Tcl1* tumor cells induce FDC networks and a tumor cell-promoting cytokine and chemokine profile in lymphopenic *Rag2*$^{-/-}$ mice.

(A) Six x 10^6 sorted *Eμ-Tcl1* cells were i.v. transferred into *Rag2*$^{-/-}$ mice (n=4). Splenic sections were stained 21 days after transfer for IgM$^+$ *Eμ-Tcl1* cells and the CD21$^+$CD35$^+$ FDC networks (upper left), for MAdCAM-1$^+$ MRCs and CXCL13 expression (upper right), for MAdCAM-1$^+$ MRCs and for CD21$^+$CD35$^+$ FDC networks (lower left), and for CD21$^+$CD35$^+$ FDC networks and CXCL13 expression (lower right). A representative section for each staining and enlarged insets of the boxed areas for CXCL13 expressing stroma cell networks are shown. Scale bars, 50 μm. (**B**) Quantitative RT-PCR of total splenic lymphotoxin (LT), TNFα, CXCL13, and BAFF transcripts in *Rag2*$^{-/-}$ mice challenged with *Eμ-Tcl1* cells (checkered bars; n=4 mice for each cytokine) or untreated (open bars; n=2-5) as a control. Transcript expression was normalized to Gapdh. Error bars indicate mean ± SEM. P values were determined by the unpaired Student's t test. *P ≤ 0.05.

Figure S9. The LTα-LTβR signaling axis is crucial for maintaining stroma cell networks and a lymphoma growth-promoting environment. (**A**) *In vivo* blockage of the LTβR signaling pathway by treatment of *Eμ-Tcl1* mice with either 100 μg LTβR-Ig (n=9; right) i.p. in 7 day intervals starting on day -1 up to day 35, or with control mouse IgG1 (MOCP21) (n=9; left). Spleens were harvested on day 38 and sections were stained for B220$^+$ B cells (blue) and BP3$^+$-follicular stromal cells (red) (upper panels), for B220$^+$ B cells (blue) and MAdCAM1$^+$ MRCs (green) (middle panels), or for B220$^+$ B cells (green) and CD31$^+$ blood vessels (red) (lower panels). A representative section of each group and staining is shown. Scale bars, 50 μm. **(B)** Tumor load in the spleen, PB, and BM of 20-27 (n=8-17), 28-39 (n=36-52), and 40-48 (n=12-51) week-old *Eμ-Tcl1* and 20-27 (n=4), 28-39 (n=5), and 40-48 (n=9) week-old *Ltα*$^{-/-}$*Eμ-Tcl1* mice was quantitated by flow cytometry analysis. Percentage of infiltrating tumor cells per organ was determined

by gating on $CD19^{+}B220^{low}CD5^{+}$ cells. Error bars indicate mean ± SEM. P values were determined by unpaired Student's *t* test. *P ≤ 0.05; **P ≤ 0.01; ***P ≤ 0.001.

Movie S1. Follicular motility of *Eμ-Tcl1* leukemia cells. Five x 10^6 labeled tumor cells were injected i.v. in C57BL/6 mice. After 16 hrs, 10 - 20 μg fluorochrome-labeled anti-$CD21^{+}CD35^{+}$ Fab-fragments were i.v. injected. Four hours after the injection of Fab-fragments, spleens were cut into 2-3 mm thick slices and transferred into a perfusion chamber. Spleen slices were imaged in a perfusion chamber. A z-stack of images consisting of 17 optical sections of 3 μm thickness was collected every 60 sec over a period of 30 min. Movie is representative of 6 mice of three independent experiments.

Movie S2. Follicular motility of B cells. Five x 10^6 labeled tumor cells or 1 x 10^7 labeled B lymphocytes were injected i.v. in C57BL/6 mice. After 16 hrs, 10 - 20 μg fluorochrome-labeled anti-$CD21^{+}CD35^{+}$ Fab-fragments were i.v. injected. Four hours after the injection of Fab-fragments, spleens were cut into 2-3 mm thick slices and transferred into a perfusion chamber. Spleen slices were imaged in a perfusion chamber. A z-stack of images consisting of 17 optical sections of 3 μm thickness was collected every 60 sec over a period of 30 min. Movie is representative of 6 mice of 5 independent experiments.

Figure S1

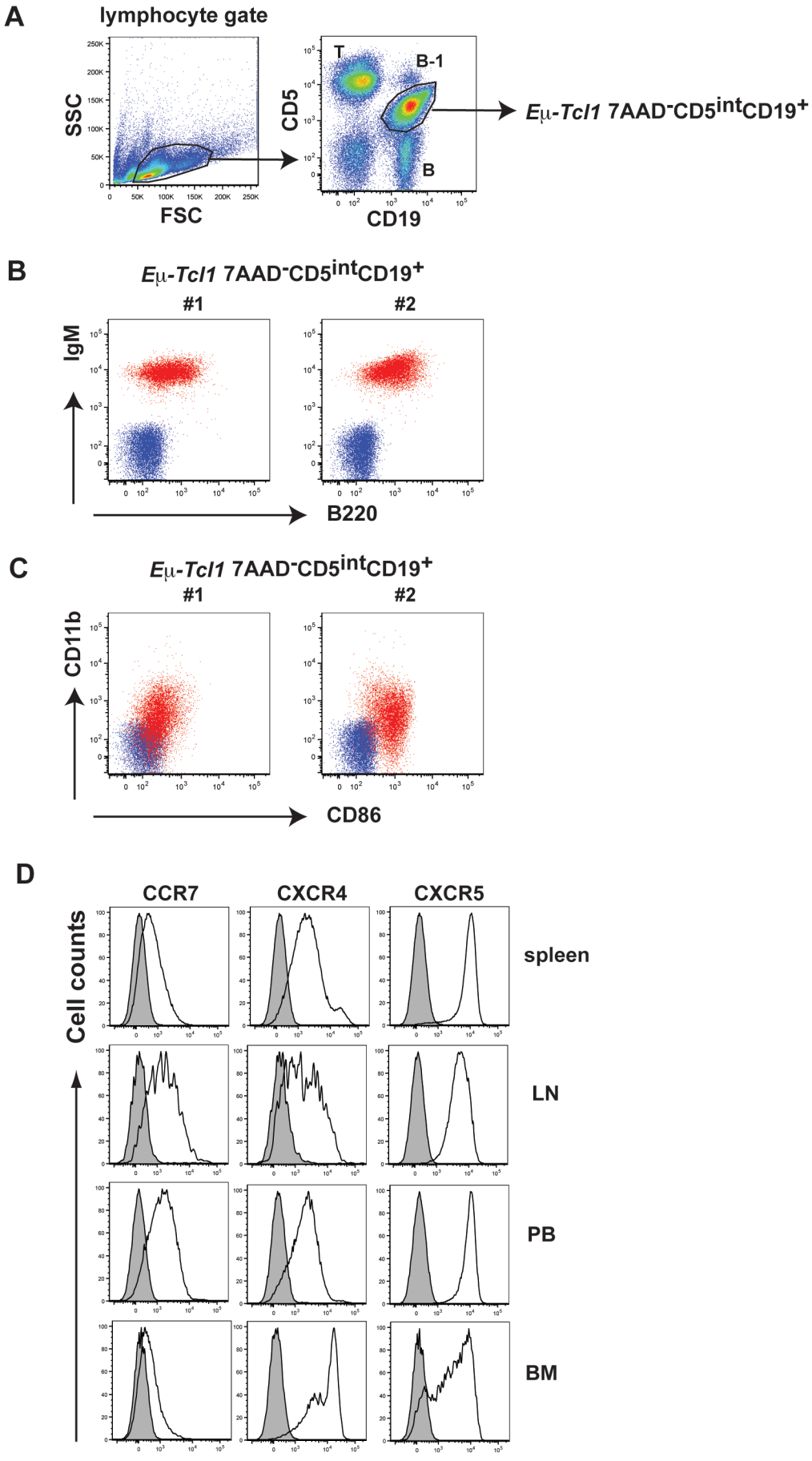
A
lymphocyte gate
SSC
FSC
CD5
CD19
T
B-1
B
Eμ-Tcl1 7AAD-CD5intCD19+
B
Eμ-Tcl1 7AAD-CD5intCD19+
#1
#2
IgM
B220
C
Eμ-Tcl1 7AAD-CD5intCD19+
#1
#2
CD11b
CD86
D
CCR7
CXCR4
CXCR5
Cell counts
spleen
LN
PB
BM

Figure S2

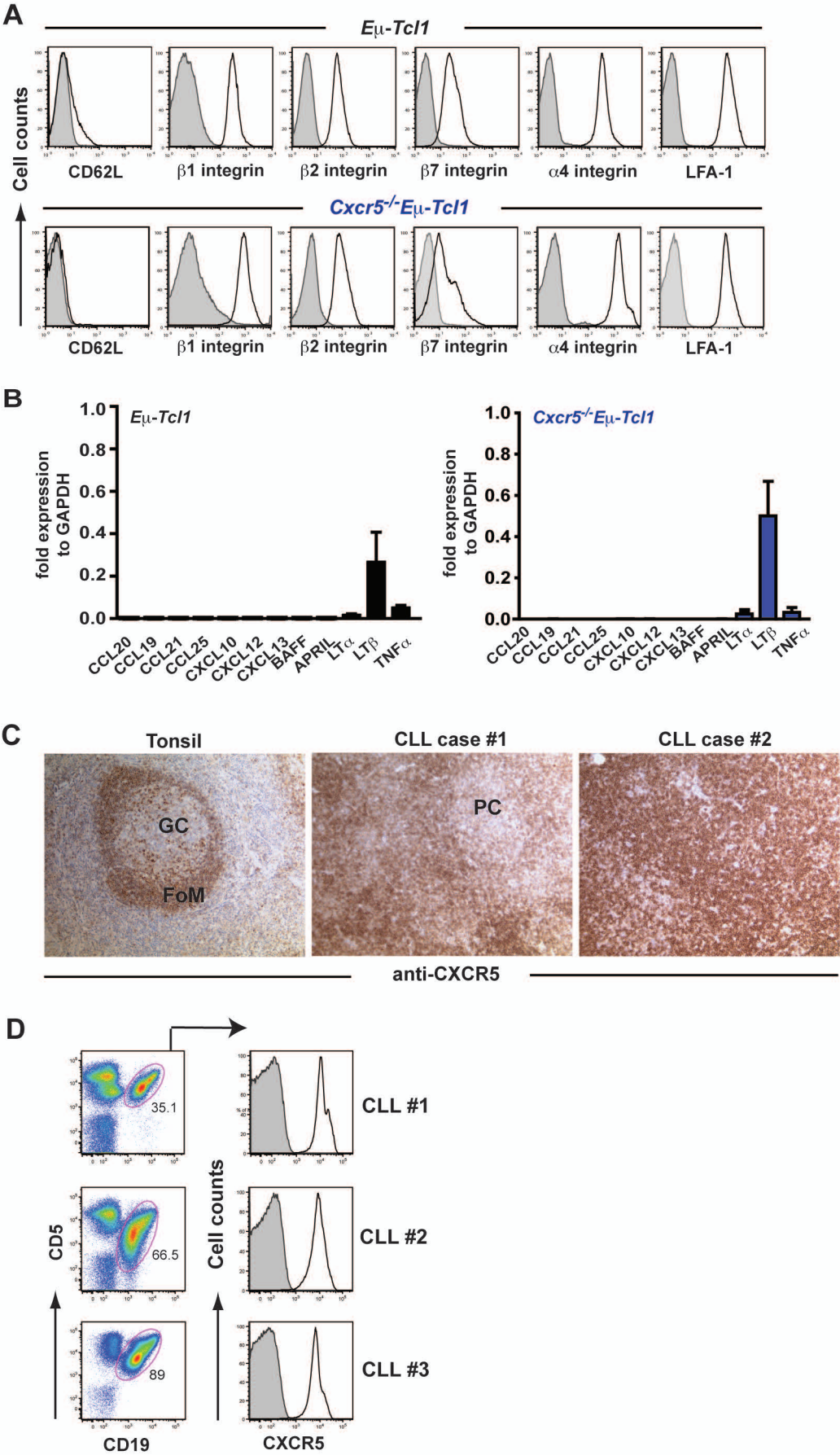
A
Eμ-Tcl1
Cell counts
CD62L
β1 integrin
β2 integrin
β7 integrin
α4 integrin
LFA-1
Cxcr5-/-Eμ-Tcl1
B
Eμ-Tcl1
fold expression to GAPDH
1.0
0.8
0.6
0.4
0.2
0.0
CCL20
CCL19
CCL21
CCL25
CXCL10
CXCL12
CXCL13
BAFF
APRIL
LTα
LTβ
TNFα
Cxcr5-/-Eμ-Tcl1
C
Tonsil
CLL case #1
CLL case #2
GC
FoM
PC
anti-CXCR5
D
35.1
66.5
89
CD5
CD19
Cell counts
CXCR5
CLL #1
CLL #2
CLL #3

Figure S3

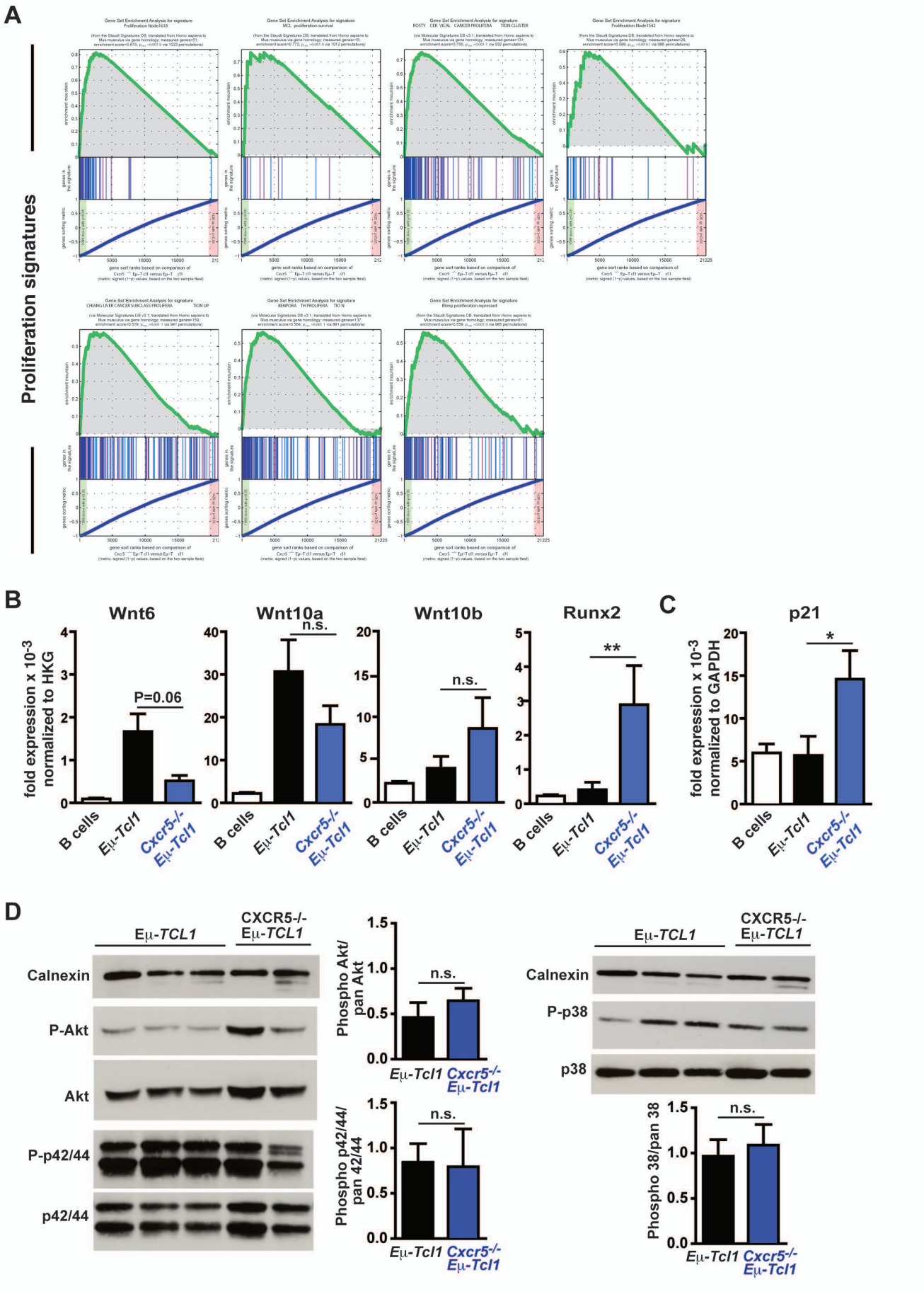
A
Proliferation signatures
B
Wnt6
Wnt10a
Wnt10b
Runx2
fold expression x 10-3 normalized to HKG
P=0.06
n.s.
**
B cells
Eμ-Tcl1
Cxcr5-/- Eμ-Tcl1
C
p21
fold expression x 10-3 normalized to GAPDH
*
D
Eμ-TCL1
CXCR5-/- Eμ-TCL1
Calnexin
P-Akt
Akt
P-p42/44
p42/44
Phospho Akt/ pan Akt
Phospho p42/44/ pan 42/44
P-p38
p38
Phospho 38/pan 38

Figure S4

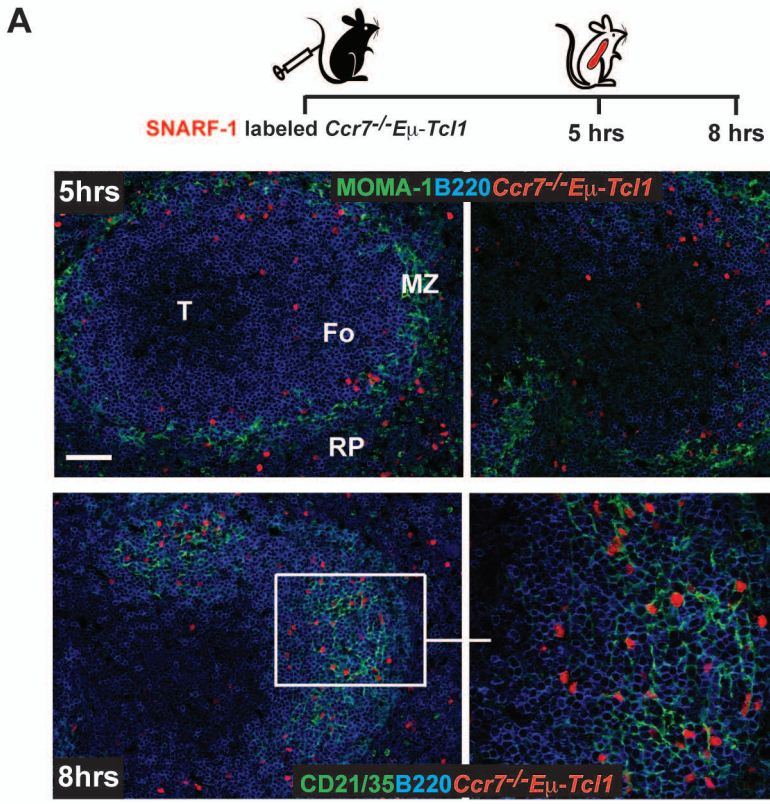
A
SNARF-1 labeled Ccr7-/-Eμ-Tcl1
5 hrs
8 hrs
5hrs
MOMA-1B220Ccr7-/-Eμ-Tcl1
8hrs
MZ
T
Fo
RP
8hrs
CD21/35B220Ccr7-/-Eμ-Tcl1

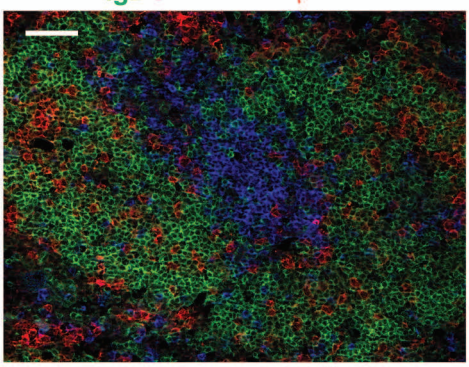
B
IgDCD3Ebi2-/-Eμ-Tcl1

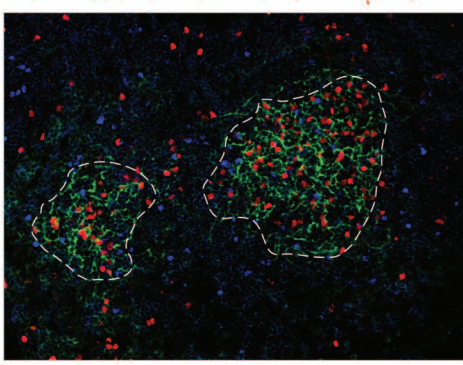
C
CD21/35FoB-CMACEbi2-/-Eμ-Tcl1

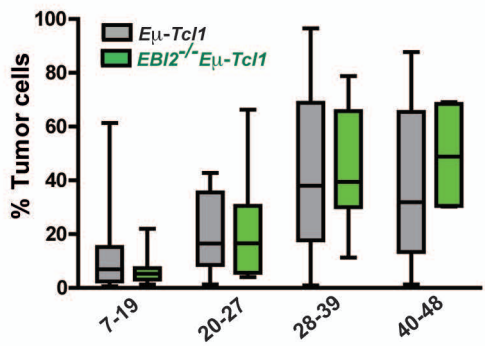
D
% Tumor cells
100
80
60
40
20
0
Eμ-Tcl1
EBI2-/-Eμ-Tcl1
7-19
20-27
28-39
40-48

Figure S5

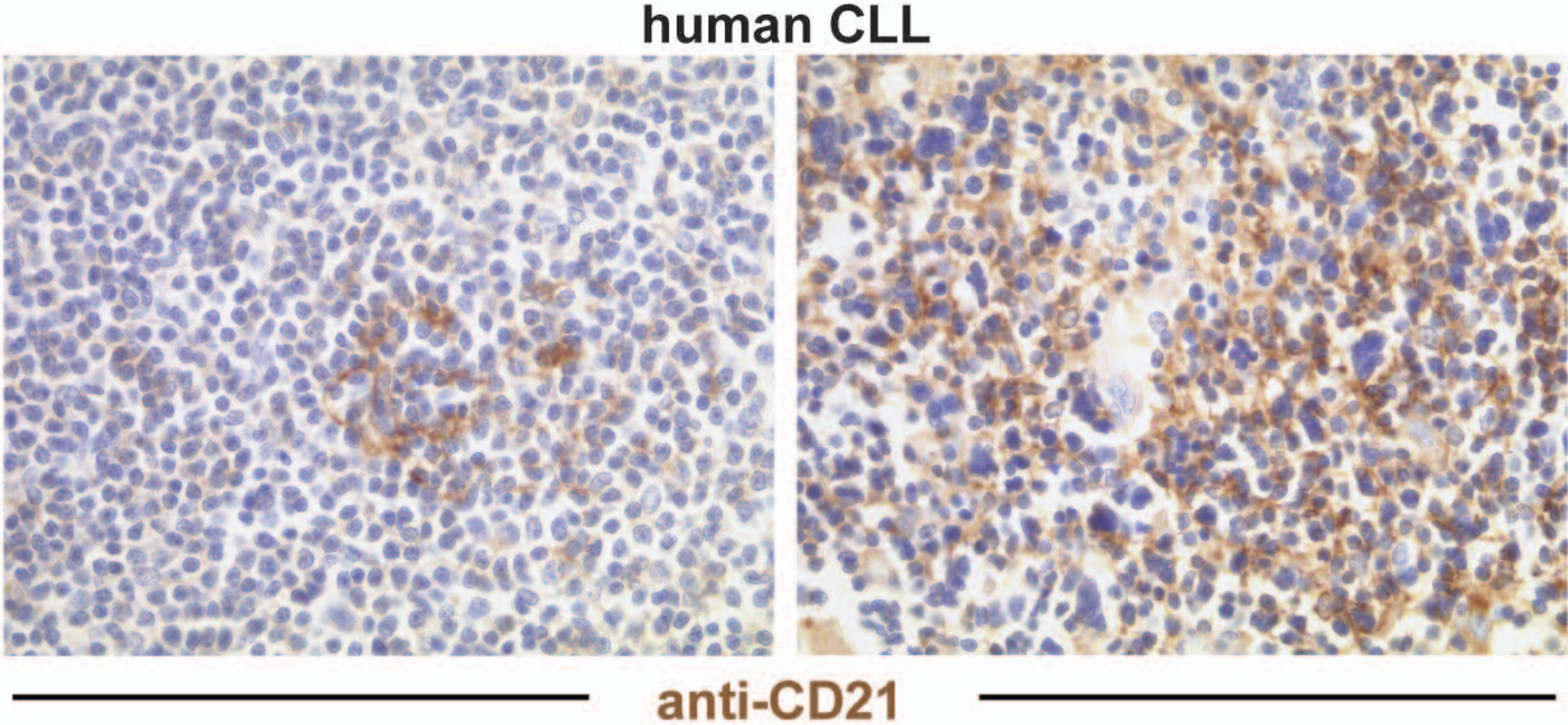

Figure S6

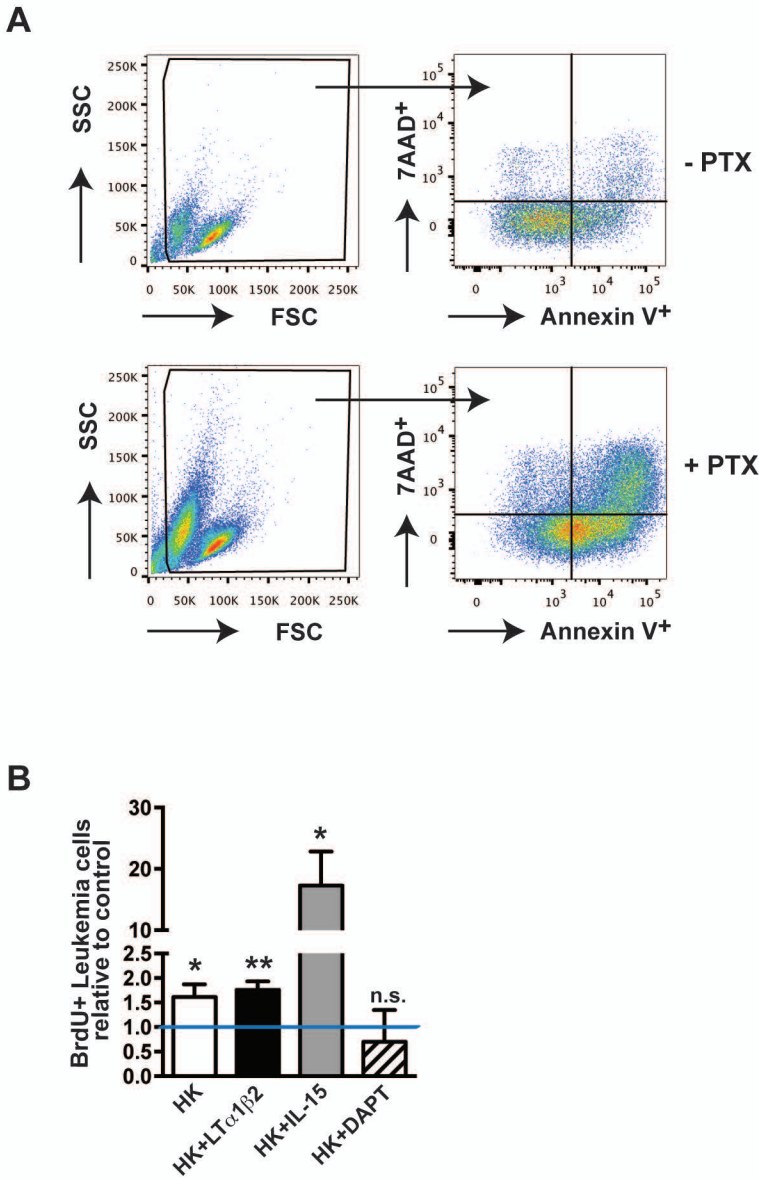
A
SSC
FSC
7AAD+
Annexin V+
- PTX
+ PTX
B
BrdU+ Leukemia cells relative to control
HK
HK+LTα1β2
HK+IL-15
HK+DAPT
n.s.

Figure S7

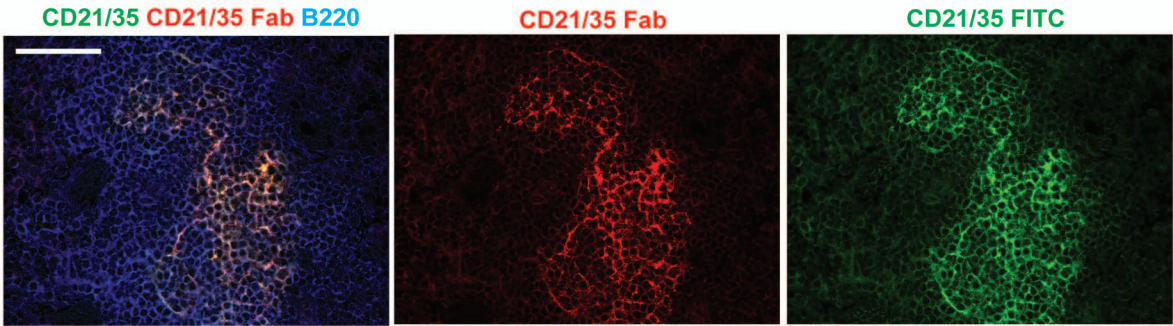

Figure S8

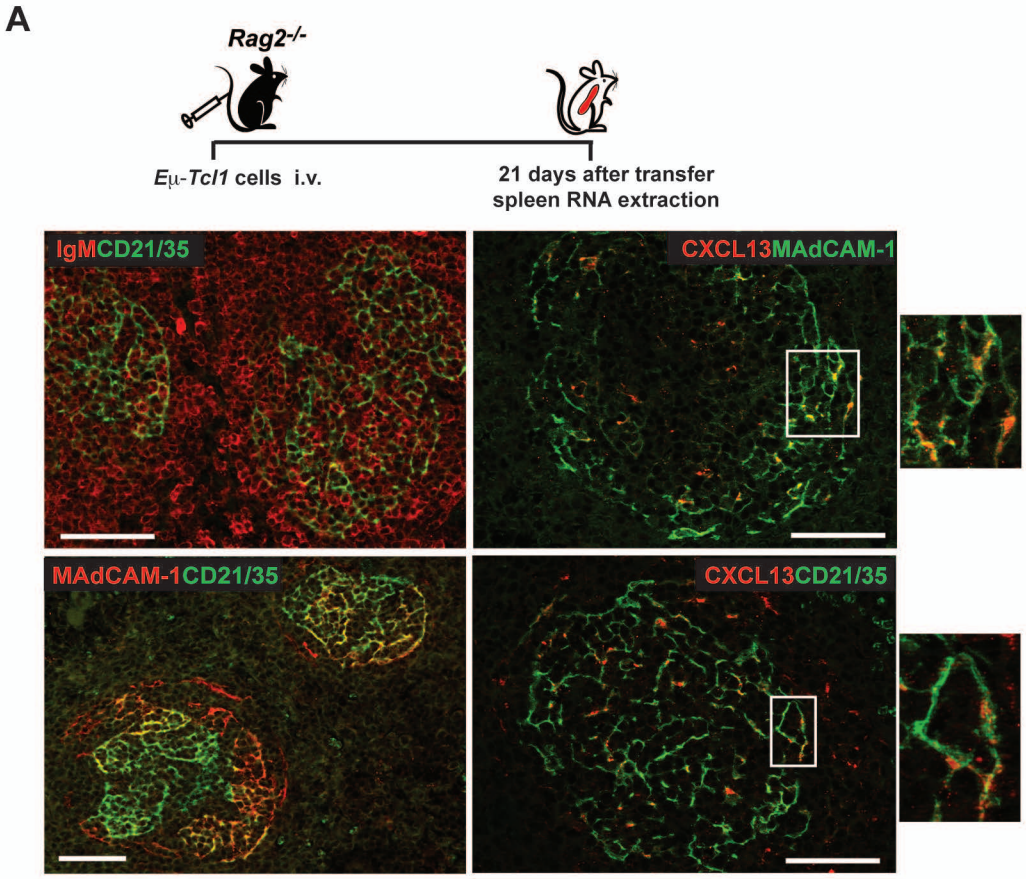
A
Rag2-/-
Eμ-Tcl1 cells i.v.
21 days after transfer
spleen RNA extraction
IgMCD21/35
CXCL13MAdCAM-1
MAdCAM-1CD21/35
CXCL13CD21/35
B
fold expression to Gapdh
0.20
0.15
0.10
0.05
0.00
Rag2-/- + Eμ-Tcl1
Rag2-/-
*
*
LTα
LTβ
TNFα
CXCL13

Figure S9

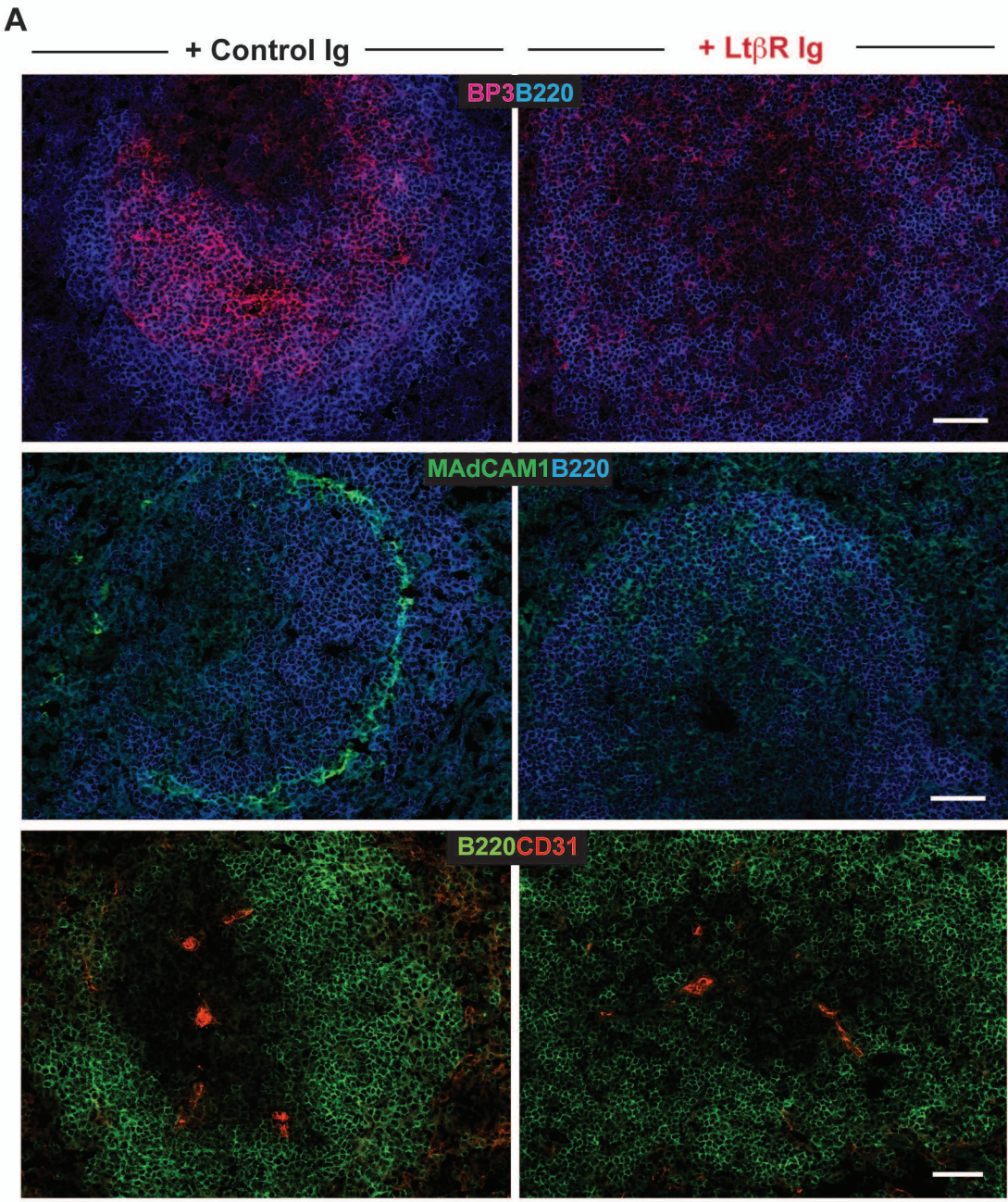
A
+ Control Ig
+ LtβR Ig
BP3B220
MAdCAM1B220
B220CD31

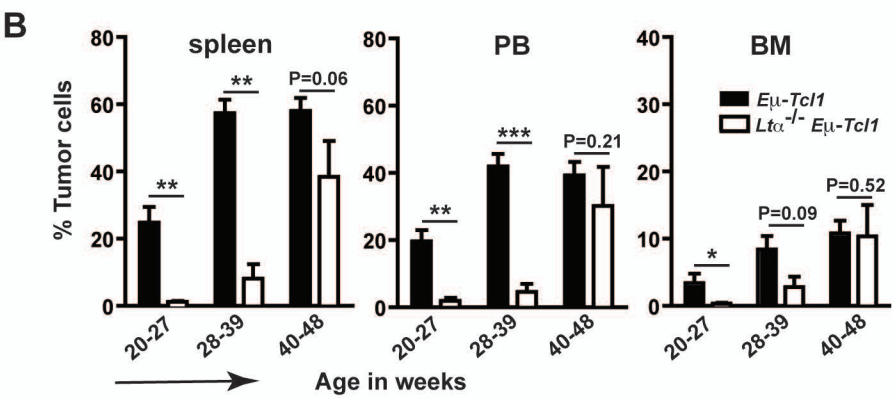
B
spleen
PB
BM
% Tumor cells
Eμ-Tcl1
Ltα-/- Eμ-Tcl1
**
**
P=0.06
**
***
P=0.21
*
P=0.09
P=0.52
20-27
28-39
40-48
Age in weeks